Studies by the U.S. Geological Survey in Alaska, 2001
U.S. Geological Survey Professional Paper 1678

A Cretaceous Ion-Microprobe U-Pb Zircon Age for the West Point Orthogneiss: Evidence for Another Gneiss Dome in the Yukon-Tanana Upland

By Cynthia Dusel-Bacon, Joseph L. Wooden, and Paul W. Layer

Abstract

We report a new ion-microprobe U-Pb zircon age of 111±2 Ma for the Orthogneiss unit of the West Point Complex (informally referred to as the West Point orthogneiss), which we interpret as the time of its igneous crystallization. Our age was determined by spot analyses of clear euhedral rims on individual zircon crystals whose faceted habit and, in some crystals, oscillatory zoning are consistent with a magmatic origin. Spot analyses of darker cores within individual zircons yielded a large population with ages of approximately 375±8 Ma and smaller populations with ages of approximately 1.1, 1.4, 1.8, and 2.6 Ga. We interpret these older cores as zircons entrained in melt derived from typical Paleozoic basement of the Yukon-Tanana Upland, which contains middle Paleozoic metaigneous rocks and abundant Precambrian inheritance in both the metaigneous and metasedimentary rocks. Our data indicate that a previously determined conventional U-Pb zircon analysis of a sample from the West Point orthogneiss that gave an upper-intercept age of 671±34 Ma actually averaged several distinct isotopic populations and thus gave a geologically meaningless age. We also determined an ion-microprobe U-Pb zircon age of 355±4 Ma for augen gneiss from the margin of the West Point Complex; this sample represents an intrusive event that probably is the source of some of the middle Paleozoic inherited zircon cores in the sample of West Point orthogneiss.

An undeformed granitic rock that crosscuts the metamorphic fabric of the sillimanite gneiss dome of the Salcha River, 30 km to the southwest, gives a preferred ion-microprobe U-Pb zircon age of 113±2 Ma. Similarities between this dome and the West Point Complex, in terms of protoliths, map scale, and proposed structural contact of the high-grade rocks with overlying greenschist-facies rocks, suggest that the West Point area is also a gneiss dome. Our new U-Pb zircon ages, together with other U-Pb and $^{40}Ar/^{39}Ar$ studies in the Yukon-Tanana Upland, indicate that mid-Cretaceous (synmetamorphic?) intrusion, metamorphism, and posttectonic intrusion all occurred within a narrow timespan. If our interpretations of mid-Cretaceous samples and their U-Pb zircon ages are correct, the maximum igneous-crystallization age of the West Point orthogneiss and the minimum igneous-crystallization age of the posttectonic Salcha River intrusion together imply that the mid-Cretaceous metamorphic episode occurred between 113 and 111 Ma.

Introduction

Amphibolite-facies metasedimentary and metaigneous rocks of continental affinity compose much of the Yukon-Tanana terrane in east-central Alaska (fig. 1). In the northern part of the Big Delta quadrangle, a 600-km^2 circular area of sillimanite gneiss, with subordinate felsic dikes, quartzite, marble, and amphibolite, forms the sillimanite gneiss dome of the Salcha River (figs. 1, 2; Dusel-Bacon and Foster, 1983). This gneissic body was subsequently referred to as the Salcha River Dome by Pavlis and others (1993) and as the Salcha River gneiss dome by Dusel-Bacon and others (2002), whose terminology we hereinafter adopt. Pavlis and others postulated that the Salcha River gneiss dome was exhumed during late Early Cretaceous regional extension. Another nearly circular, ~150-km^2 area of high-grade gneiss and metasedimentary rocks, the main subject of this chapter, crops out approximately 75 km northeast of the center of the Salcha River gneiss dome, in a topographically high area that includes 5,865-ft-high West Point peak (figs. 1, 2). This complex, referred to as the West Point Complex by Smith and others (1994), consists of peraluminous granitic orthogneiss, sillimanite gneiss, quartzite, and marble. The peraluminous orthogneiss (Orthogneiss unit of the West Point Complex of Smith and others, 1994; hereinafter referred to as the West Point orthogneiss) lies in the core of a metaigneous and high-grade metamorphic complex in the northeastern part of the Big Delta quadrangle that forms the core of an east-west-trending antiform (Smith and others, 1994).

Medium-grained biotite-muscovite granitic orthogneiss from the core of the West Point Complex was previously sampled for U-Pb zircon dating in 1983 during an Alaska Division of Geological and Geophysical Surveys mapping project in the upper Chena River area (Smith and others, 1994). Ther-

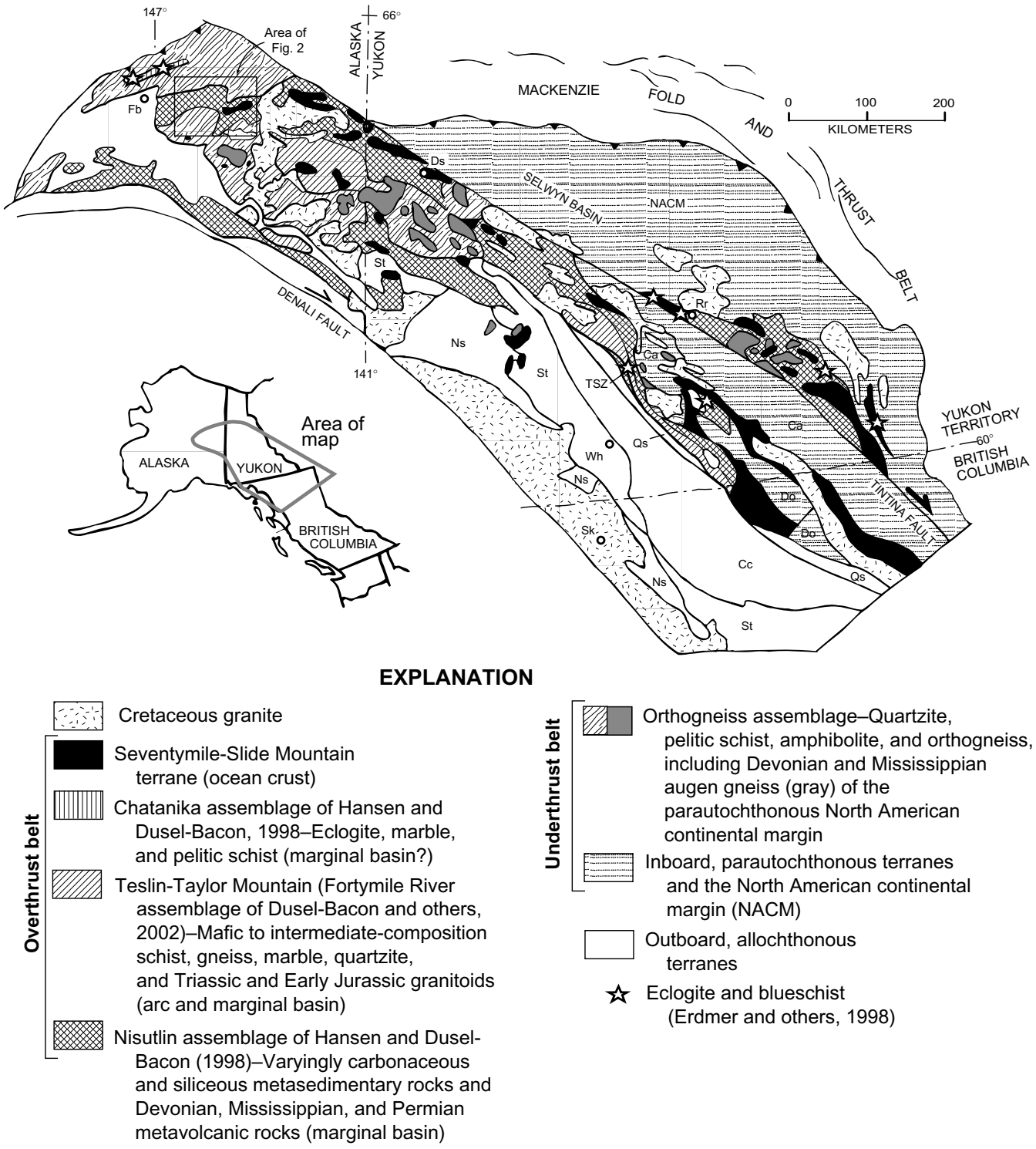

Figure 1. Simplified terrane and tectonic assemblage map of northern Canadian and the Alaskan Cordillera (modified from Hansen and others, 1991, and Dusel-Bacon and Cooper, 1999). Towns (circles): Ds, Dawson; Fb, Fairbanks; Rr, Ross River; Sk, Skagway; Wh, Whitehorse. Terranes: Ca, Cassiar; Cc, Cache Creek; Do, Dorsey; Ns, Nisling; Qs, Quenellia; St, Stikinia. Unlabeled area surrounding Fairbanks is alluvium of the Tanana River Valley; unlabeled area adjacent to north side of the Denali Fault in Alaska comprises various terranes not discussed in this chapter. Tertiary granitoids not shown. The Yukon-Tanana Upland physiographic province in Alaska includes all the area north of the Tanana River Valley; units above that are included in the broadly defined "Yukon-Tanana terrane" are the Chatinika assemblage of Hansen and Dusel-Bacon (1998; equivalent to unit ec of Foster and others, 1994), the Fortymile River assemblage of Dusel-Bacon and others (2002), the Nisutlin assemblage of Hansen and Dusel-Bacon (1998), and the orthogneiss assemblage of Hansen and Dusel-Bacon (1998).

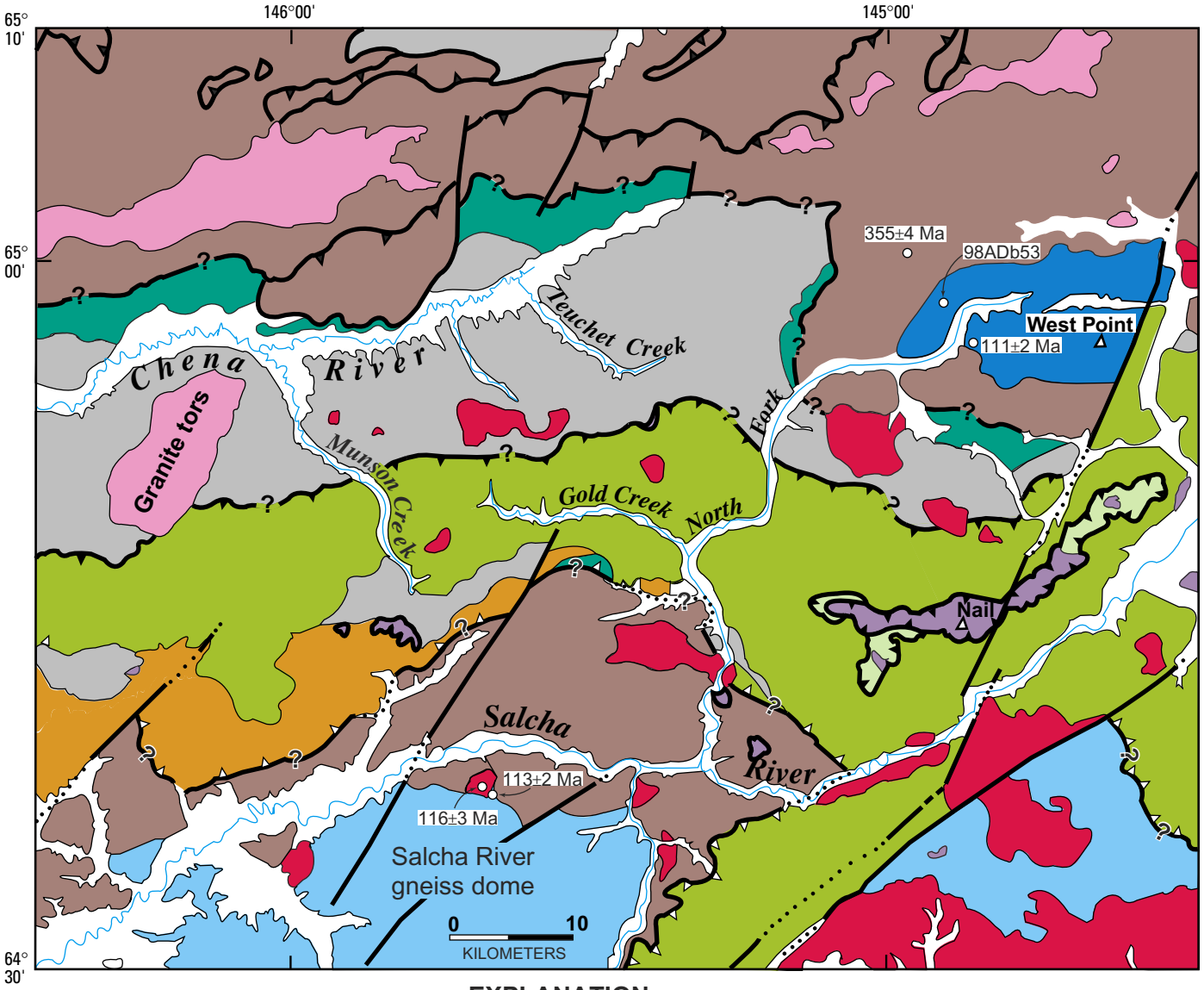

EXPLANATION

- Surficial deposits (Quaternary)
- Postmetamorphic granitoids (Tertiary and Cretaceous)

STRUCTURALLY HIGHER ROCKS

- Peridotite (purple), greenstone, metalimestone, metachert, and metasedimentary rocks (Triassic, Permian, and Mississippian–Seventymile terrane)
- Greenschist-facies semischist, phyllite, quartzite, marble, and greenstone (Mississippian and Devonian)–Butte subterrane of the Yukon-Tanana terrane of Pavlis and others (1993)
- Greenschist-facies quartzofeldspathic mylonite schist and gneiss (Mississippian and Devonian)

STRUCTURALLY LOWER ROCKS

- Greenschist-facies carbonaceous quartzite and phyllite and felsic and mafic metavolcanic rocks (Mississippian and Devonian)–Nasina assemblage of Wheeler and McFeely (1991)
- Amphibolite-facies calcareous phyllite and marble
- Amphibolite-facies peltic schist, quartzite, marble, and amphibolite
- Amphibolite-facies sillimanite gneiss, quartzite, and marble
- Amphibolite-facies quartzite, marble, pelitic schist, and orthogneiss–West Point Complex of Smith and others (1994)

- Contact
- Fault; dotted where concealed
- Thrust fault; sawteeth on upper plate, queried where uncertain
- Low-angle normal fault; sawteeth on upper plate, dotted where concealed, queried where uncertain
- Sample site
- Named Peak

Figure 2. Geologic map of the northern part of the Big Delta quadrangle (south of lat 65° N.) and the southern Circle quadrangle (north of lat 65° N.) (modified from Weber and others, 1978, and Foster, 1992, respectively), showing locations of sample sites discussed in text.

mal-ionization mass-spectrometric (TIMS) analyses of five multigrain zircon fractions yielded a highly discordant array. A discordia chord plotted through the array gave an upper-intercept age of 671±34 Ma (Late Proterozoic) that Smith and others interpreted as the time of igneous crystallization of the orthogneiss; they concluded that the metapelitic and metapsammitic wallrocks, which they correlated with the Fairbanks schist unit of Robinson and others (1990), had a Late Proterozoic minimum depositional age. Monazite separated from the orthogneiss that yielded the Late Proterozoic upper-intercept age gave a concordant U-Pb age of 115 Ma (Smith and others, 1994).

Owing to the importance of the Late Proterozoic crystallization age proposed for the granitic orthogneiss (which led Smith and others, 1994, to designate the entire West Point Complex and adjacent quartzite-dominant basement rocks as Precambrian) and the high degree of Pb loss reflected in the extreme discordance of the U-Pb zircon data, we resampled the orthogneiss at the same locality as the previously collected sample. Because of the possible presence of inherited, xenocrystic cores within igneous zircons, this second collection of zircons was dated by using the sensitive high-resolution ion microprobe (SHRIMP) that analyzes ~30-µm-diameter areas, resulting in ages for both inherited cores and magmatic rims. In addition to redating the orthogneiss, we carried out SHRIMP U-Pb geochronology on a sample of augen gneiss that intrudes the pelitic schist unit flanking the orthogneiss core of the West Point Complex, as well as on a granitic sample from a postkinematic granitoid body that intrudes the Salcha River gneiss dome to the southwest. To address the cooling history of the West Point orthogneiss, we also determined $^{40}Ar/^{39}Ar$ ages for biotite and white mica from the same sample as that used for U-Pb geochronology.

Regional Tectonic Framework

The Yukon-Tanana Upland of east-central Alaska and the Yukon Territory, Canada (fig. 1), consists of thrust sheets of ductilely deformed metasedimentary and metaigneous assemblages of uncertain age and origin that are overlain by klippen of weakly metamorphosed oceanic rocks of the Seventymile-Slide Mountain terrane and are intruded by postkinematic Early Jurassic, Cretaceous, and Tertiary granitoids (Foster and others, 1994). The ductilely deformed metamorphic assemblages have commonly been referred to as the Yukon-Tanana terrane (for example, Coney and others, 1980; Mortensen, 1992), a term used to collectively describe the broad band of heterogeneous metamorphic assemblages that lies between the right-lateral Denali and Tintina Fault zones in east-central Alaska and the Yukon Territory (fig. 1). A flap of this heterogeneous province has been dextrally offset by approximately 450 km along the Tintina Fault and now lies northeast of the fault. Several studies (for example, Churkin and others, 1982; Foster and others, 1985; Aleinikoff and others, 1987; Hansen, 1990) have shown that these assemblages have different geologic histories.

On the basis of protolith assemblages and pluton distribution, structural and kinematic data, metamorphic pressure-temperature data, and metamorphic-cooling ages, the following tectonic history has been proposed (Hansen and others, 1991; Dusel-Bacon and others, 1995, 2002; Hansen and Dusel-Bacon, 1998). Upper-plate assemblages—peridotite, greenstone, and Mississippian to Triassic metasedimentary rocks of the Seventymile terrane; eclogitic rocks of the Chatinika assemblage (terminology of Hansen and Dusel-Bacon, 1998; equivalent to unit ec of Foster and others, 1994) of the Yukon-Tanana terrane; and amphibolite-facies gneiss, amphibolite, marble, and metachert of the Fortymile River assemblage of Dusel-Bacon and others (2002)—were affected by pre-Jurassic, northeastward-directed, apparent margin-normal crustal contraction, interpreted to have occurred during west-dipping subduction before their emplacement onto lower-plate continental-margin rocks (including Paleozoic protoliths of the West Point Complex). Greenschist-facies siliciclastic and volcanic rocks (Nisutlin terrane, fig. 1) occur at intermediate structural levels. The association of rocks of the Nisutlin terrane with oceanic rocks of the Seventymile terrane, and the fact that Late Triassic and Early Jurassic granitoids intrude both the Fortymile River assemblage and the Nisutlin terrane in the eastern Yukon-Tanana Upland but are absent in lower-plate assemblages, suggest an allochthonous origin for the Nisutlin terrane as well. Amphibolite-facies marginal-basin schist, gneiss, and quartzite of continental affinity and peraluminous to metaluminous Devonian and Mississippian orthogneiss, commonly augen gneiss, that occur at the lowest structural level—the Lake George assemblage of Dusel-Bacon and Cooper (1999), the Chena River sequence of Smith and others (1994), and the Fairbanks schist unit—are interpreted to be parautochthonous to the early to middle Paleozoic continental margin of North America. Early and Middle Jurassic (>188–185 Ma) northwestward-directed, apparent margin-parallel crustal contraction and imbrication resulted in crustal thickening and tectonic burial of lower-plate assemblages and a northwestward-vergent penetrative fabric shared by both upper- and lower-plate assemblages. Subsequent Early Cretaceous (135–110 Ma) tectonism was widespread throughout the Yukon-Tanana Upland. In some areas, particularly in the eastern part of the upland and bordering the Salcha River gneiss dome, Early Cretaceous cooling appears to have accompanied southeastward-directed crustal extension that resulted in exposure of the structurally deepest parautochthonous continental rocks (Hansen and others, 1991; Pavlis and others, 1993; Hansen and Dusel-Bacon, 1998). In other areas, however, such as in the southeastern part of the Big Delta quadrangle, Early Cretaceous metamorphic cooling ages are not associated with southeastward-vergent deformation, and so the Early Cretaceous tectonism in those areas may have resulted from crustal contraction rather than extension (Day and others, 2002; Dusel-Bacon and others, 2002).

Local Geology

The gneiss, quartzite, and marble in the core of the West Point Complex are successively overlain by (1) a unit of amphibolite-facies pelitic schist, quartzite, marble, amphibolite, and small bodies and sills (3-m-thick concordant layers) of augen gneiss; (2) calcareous phyllite and marble; and (3) varyingly carbonaceous, siliceous, and calcareous quartzite and phyllite and minor felsic and mafic greenschist-facies metavolcanic rocks (fig. 2; Weber and others, 1978; Smith and others, 1994). Metamorphic grade in the amphibolite-facies rocks ranges from the staurolite zone to the sillimanite zone (Dusel-Bacon and others, 1989, 1993). In the southeastern part of the Circle quadrangle, the maximum metamorphic grade appears to be close to the muscovite+quartz=sillimanite+K-feldspar+water isograd (Foster and others, 1983), indicating peak temperatures of about 600–650°C (Chatterjee and Johannes, 1974). A sample of augen gneiss from a small body that intrudes the northern margin of the pelitic schist unit north of the headwaters of the Salcha River along the north flank of the West Point Complex yielded a conventional (TIMS) U-Pb zircon age of approximately 340 Ma (Foster and others, 1987). This age, interpreted as the approximate igneous-crystallization age of the augen gneiss, is the upper-intercept age of a discordia line drawn through two fine-grained zircon fractions and slightly above a third fine-grained fraction. This stratigraphic sequence in the greater West Point area is nearly the same as that overlying the sillimanite gneiss unit of the Salcha River gneiss dome. A greenschist-facies semischist unit (noncarbonaceous part of the Nisutlin assemblage of Hansen and Dusel-Bacon, 1998; referred to as the Butte subterrane of the Yukon-Tanana terrane by Pavlis and others, 1993, and hereinafter as the Butte assemblage) overlies both high-grade areas along a poorly exposed contact interpreted as a low-angle fault, but the sense of motion along the fault is open to speculation (Dusel-Bacon and others, 1993; Pavlis and others, 1993; Foster and others, 1994; Smith and others, 1994).

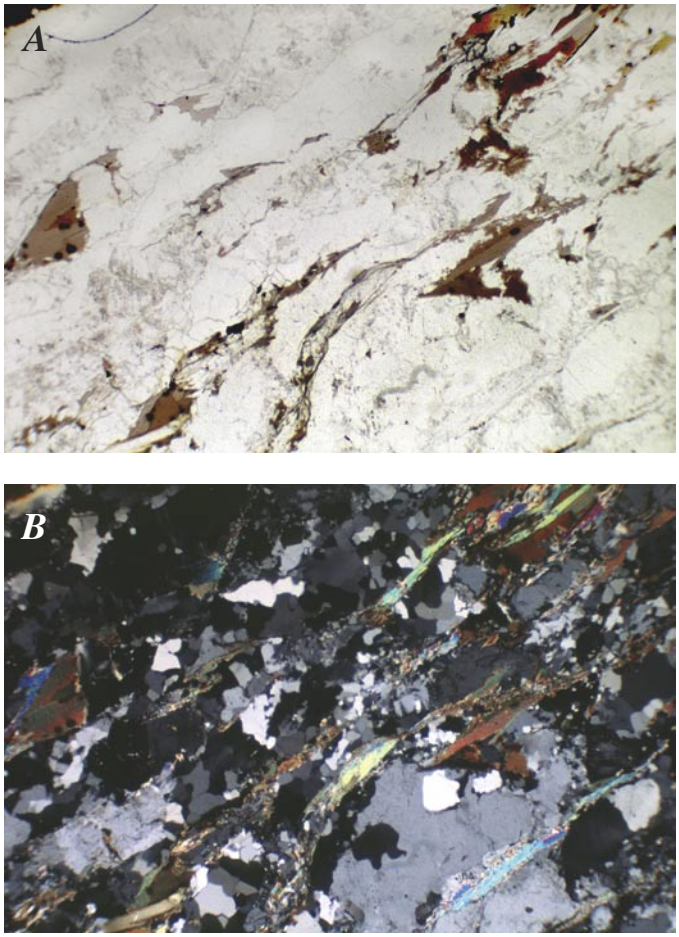

Figure 3. Photomicrograph of sample 96ADb10A of West Point orthogneiss (tables 1-4) taken with transmitted light (*A*) and crossed polars (*B*). Note alignment of thin biotite and muscovite grains; in figure 3*B*, muscovite is yellow, green, and pink, biotite is brown, K-feldspar is light gray, and quartz is black or white, depending on orientation of quartz grains.

Geochronology

Description of Geochronology Samples

Sample 96ADb10A (tables 1–4) is a quartz–K-feldspar–plagioclase–muscovite–biotite orthogneiss. The moderately well developed foliation is defined by aligned micas and elongate feldspar grains (fig. 3). Quartz grains are primarily annealed, with only weak undulatory extinction and lattice preferred orientation, suggesting that recrystallization of quartz outlasted most of the deformation. No evidence of retrograde metamorphism was observed. Trace amounts of apatite, chlorite, zircon, titanite, and Fe-Ti oxides are present. The sample was collected from one of the large blocks of homogeneous orthogneiss rubble that make up one of the steep peaks, along a glaciated ridge west of West Point (fig. 2). To ensure that we sampled the same rock which had previously yielded the highly discordant TIMS U-Pb zircon upper-intercept age of 671±34 Ma, the first author obtained a hand specimen from the exact site of the previously sampled rock.

Sample 98ADb55B (tables 1, 4) is a quartz-biotite-microcline-plagioclase augen gneiss. Although the gneiss has a well-developed foliation, petrographic examination reveals that the quartz forms sub-millimeter-thick layers (parallel to foliation) and exhibits straight grain boundaries and uniform extinction, indicating annealing. The sample was collected from a large block below an outcrop of augen gneiss within the pelitic schist unit (fig. 2; Chena River sequence of Smith and others, 1994).

Sample 98ADb66B (tables 1, 4) is a hypidiomorphic-granular, medium-grained granite. K-feldspar is approximately equal in abundance to plagioclase; the rock contains minor biotite, some of which has been altered to chlorite, and trace amounts of Fe-Ti oxides. No alignment of mica or feldspars was observed to suggest foliation. The only evidence of deformation is quartz straining, manifested as patchy to undulose extinction. The sample was collected from an ~70-cm-thick granitic dike that crosscuts the foliation of sillimanite gneiss at the northern

Table 1. U-Pb geochronologic data for (meta)igneous rocks of the West Point Complex and Salcha River gneiss dome.

[All ages in millions of years. Spot analyses are listed in order of increasing $^{206}Pb/^{238}U$ age. cr, correction for common Pb by either ^{204}Pb or ^{207}Pb method, as indicated; err corr, error correction; r (after isotope number), radiogenic]

Spot name	Spot position	U (ppm)	Th (ppm)	$^{232}Th/^{238}U$ ratio	^{207}Pb-cr $^{206}Pb/^{238}U$ age	1σ age	^{204}Pb-cr $^{206}Pb/^{238}U$ age	1σ age	^{204}Pb-cr $^{207}Pb/^{235}U$ age	1σ age	^{204}Pb-cr $^{207}Pb/^{206}Pb$ age	1σ age	^{207}Pb-cr ^{206}Pb-r/^{238}U ratio	1σ	Total $^{238}U/^{206}Pb$ ratio	1σ	Total $^{207}Pb/^{206}Pb$ ratio	Error (pct)	^{204}Pb-cr $^{238}U/^{206}Pb$-r	Error (pct)	^{204}Pb-cr ^{207}Pb-r/^{206}Pb-r	Error (pct)	^{204}Pb-cr ^{207}Pb-r/^{235}U	Error (pct)	^{204}Pb-cr ^{206}Pb-r/^{238}U	Error (pct)	err corr
Sample 96ADb10A																											
10—7.1	r	759	703	0.96	101.5	1.6	100.1	1.7	77.6	14.0	— —	— —	0.0159	0.0002	62.28	1.5	0.0570	2.6	63.88	1.7	0.0368	18.8	0.079	18.9	0.0157	1.7	0.092
10—9.1	r	775	68	.09	104.8	1.6	105.2	1.6	111.8	2.9	— —	— —	.0164	.0003	60.79	1.5	.0513	2.3	60.79	1.5	.0513	2.3	.116	2.8	.0165	1.5	.552
10—1.1	r	1,448	211	.15	110.0	1.6	109.8	1.6	106.8	2.7	— —	— —	.0172	.0002	57.98	1.4	.0496	1.6	58.19	1.4	.0468	2.2	.111	2.6	.0172	1.4	.543
10—4.1	r	1,278	102	.08	110.5	1.6	109.9	1.6	100.0	4.9	— —	— —	.0173	.0003	57.73	1.5	.0497	1.7	58.17	1.5	.0437	5.0	.104	5.2	.0172	1.5	.284
10—5.1	r	1,434	153	.11	110.0	1.6	110.2	1.6	112.7	3.5	— —	— —	.0172	.0002	58.16	1.4	.0475	1.7	58.02	1.5	.0494	3.0	.117	3.3	.0172	1.5	.438
10—2.1	r	1,322	246	.19	112.2	1.6	111.2	1.6	96.4	2.6	— —	— —	.0176	.0003	57.13	1.4	.0461	2.2	57.46	1.4	.0415	2.5	.100	2.9	.0174	1.4	.501
10—8.1	r	1,114	68	.06	111.5	1.8	111.4	1.8	111.0	5.4	— —	— —	.0174	.0003	57.22	1.6	.0498	1.9	57.35	1.6	.0480	4.9	.116	5.1	.0174	1.6	.312
10—3.1	r	5,387	67	.01	114.1	1.6	113.8	1.5	109.1	2.1	— —	— —	.0179	.0002	56.02	1.4	.0480	.8	56.15	1.4	.0462	1.6	.113	2.1	.0178	1.4	.661
10—26.1	r	3,019	651	.22	115.1	1.6	114.9	1.6	112.6	2.0	— —	— —	.0180	.0002	55.55	1.4	.0478	.8	55.58	1.4	.0473	1.2	.117	1.8	.0180	1.4	.749
10—33.1	r	7,064	235	.03	121.4	1.6	121.3	1.6	120.1	2.1	— —	— —	.0190	.0003	52.59	1.4	.0485	1.1	52.63	1.4	.0479	1.3	.126	1.9	.0190	1.4	.727
10—10.1	r	5,339	176	.03	121.7	1.7	121.5	1.7	118.8	2.0	— —	— —	.0191	.0003	52.49	1.4	.0480	.8	52.54	1.4	.0473	1.2	.124	1.8	.0190	1.4	.755
10—31.1	r	7,771	132	.02	125.9	1.7	125.9	1.7	124.7	1.8	— —	— —	.0197	.0003	50.70	1.4	.0485	.5	50.72	1.4	.0481	.7	.131	1.5	.0197	1.4	.891
10—6.1	r	5,721	532	.10	128.8	1.7	128.7	1.7	126.4	2.0	— —	— —	.0202	.0003	49.51	1.4	.0492	.7	49.61	1.4	.0477	.9	.133	1.6	.0202	1.4	.829
10—5.2	c	1,317	75	.06	219.1	3.1	222.3	3.1	266.5	5.1	— —	— —	.0346	.0005	28.46	1.4	.0633	1.2	28.51	1.4	.0620	1.6	.300	2.2	.0351	1.4	.655
10—30.1	c	1,722	591	.35	267.3	3.7	267.7	3.6	272.7	4.1	— —	— —	.0423	.0006	23.57	1.4	.0530	.7	23.58	1.4	.0527	1.0	.308	1.7	.0424	1.4	.800
10—8.2	c	729	161	.23	304.6	4.8	304.4	4.7	301.5	7.8	— —	— —	.0484	.0008	20.63	1.6	.0540	1.4	20.68	1.6	.0519	2.5	.346	3.0	.0484	1.6	.531
10—1.2	c	719	269	.39	327.0	4.6	326.3	4.5	317.2	5.7	— —	— —	.0520	.0008	19.18	1.4	.0545	1.2	19.26	1.4	.0512	1.5	.367	2.1	.0519	1.4	.679
10—23.2	r	445	116	.27	338.7	5.3	339.0	5.2	343.3	7.6	— —	— —	.0539	.0009	18.52	1.6	.0542	2.1	18.52	1.6	.0540	2.1	.402	2.6	.0540	1.6	.600
10—25.1	c	218	102	.48	353.6	5.4	353.8	5.5	355.8	15.8	— —	— —	.0564	.0009	17.68	1.6	.0559	1.8	17.73	1.6	.0540	5.1	.420	5.3	.0564	1.6	.300
10—32.1	r	947	344	.38	354.8	4.9	355.1	4.8	359.2	4.8	— —	— —	.0566	.0008	17.66	1.4	.0541	.8	17.66	1.4	.0543	.8	.424	1.6	.0566	1.4	.868
10—28.1	c	1,586	476	.31	361.3	4.9	361.1	4.8	358.6	4.8	— —	— —	.0577	.0008	17.33	1.4	.0543	.6	17.35	1.4	.0533	.8	.424	1.6	.0576	1.4	.863
10—24.1	c	590	230	.40	362.4	5.1	362.3	5.0	360.7	7.7	— —	— —	.0578	.0008	17.26	1.4	.0551	1.0	17.30	1.4	.0535	2.1	.427	2.6	.0578	1.4	.559
10—34.1	r	1,729	547	.33	370.5	5.0	370.5	5.0	370.4	7.0	— —	— —	.0592	.0008	16.88	1.4	.0552	1.5	16.90	1.4	.0540	1.8	.440	2.3	.0592	1.4	.611
10—29.1	c	227	167	.76	371.9	5.7	371.4	5.6	364.8	8.3	— —	— —	.0594	.0009	16.81	1.5	.0555	1.6	16.86	1.5	.0529	2.3	.432	2.7	.0593	1.5	.566
10—12.1	c	650	259	.41	374.1	5.6	372.1	5.5	346.9	7.1	— —	— —	.0597	.0009	16.76	1.5	.0529	1.7	16.83	1.5	.0497	1.9	.407	2.4	.0594	1.5	.626
10—6.2	c	529	300	.59	378.2	5.4	377.3	5.4	365.4	10.3	— —	— —	.0604	.0009	16.55	1.5	.0540	1.4	16.59	1.5	.0521	3.0	.433	3.4	.0603	1.5	.435
10—21.1	c	148	67	.47	383.6	7.3	382.5	7.2	368.8	18.2	— —	— —	.0613	.0012	16.27	1.9	.0562	3.4	16.36	1.9	.0520	5.6	.438	5.9	.0611	1.9	.326
10—22.1	c	1,517	475	.32	387.8	5.4	387.0	5.3	376.5	5.7	— —	— —	.0620	.0009	16.12	1.4	.0548	1.1	16.16	1.4	.0526	1.1	.449	1.8	.0619	1.4	.785
10—23.1	c	896	496	.57	391.7	5.6	390.9	5.6	380.5	11.8	— —	— —	.0626	.0009	15.95	1.5	.0551	1.3	16.00	1.5	.0528	3.4	.455	3.7	.0625	1.5	.392
10—16.1	c	791	862	1.13	401.5	6.1	401.3	6.0	399.1	7.5	— —	— —	.0643	.0010	15.55	1.5	.0552	1.5	15.57	1.5	.0544	1.7	.481	2.3	.0642	1.5	.675
10—2.2	c	1,236	779	.65	402.5	5.6	407.5	5.6	467.0	7.9	771	33.4	.0644	.0009	15.30	1.4	.0660	.8	15.33	1.4	.0649	1.6	.584	2.1	.0653	1.4	.663
10—27.1	c	493	77	.16	450.9	6.4	488.4	6.8	849.1	9.8	1,964	16.4	.0725	.0011	12.68	1.4	.1221	.8	12.71	1.4	.1205	.9	1.308	1.7	.0787	1.4	.843
10—20.1	c	526	265	.52	469.8	7.3	487.9	8.1	678.5	30.4	1,376	115.2	.0756	.0012	12.35	1.6	.1102	1.2	12.72	1.7	.0877	6.0	.951	6.2	.0786	1.7	.275
10—15.1	c	530	148	.29	743.5	10.8	845.9	11.7	1,481.1	12.7	2,564	12.0	.1223	.0019	7.13	1.5	.1713	.7	7.13	1.5	.1707	.7	3.300	1.6	.1402	1.5	.900
10—14.1	c	33	13	.41	825.3	22.7	872.1	22.9	1,206.1	30.3	1,866	60.4	.1366	.0040	6.90	2.8	.1141	3.3	6.90	2.8	.1141	3.3	2.280	4.4	.1449	2.8	.642
10—17.1	c	306	79	.27	1,088.7	19.3	1,067.8	15.5	905.7	87.3	— —	— —	.1840	.0035	5.52	1.6	.0629	13.4	5.55	1.6	.0580	15.1	1.440	15.2	.1802	1.6	.103
10—3.2	c	80	59	.76	1,179.8	20.1	1,178.8	19.1	1,172.8	18.9	1,162	41.6	.2008	.0038	4.97	1.8	.0806	1.7	4.98	1.8	.0786	2.1	2.174	2.7	.2007	1.8	.645
10—11.1	c	245	122	.52	1,691.4	25.9	1,704.6	23.6	1,757.7	16.5	1,821	22.0	.3000	.0052	3.30	1.6	.1128	.9	3.30	1.6	.1113	1.2	4.646	2.0	.3027	1.6	.792
10—13.1	c	65	39	.62	1,877.2	38.6	1,875.7	33.9	1,870.0	24.6	1,864	36.9	.3380	.0080	2.96	2.1	.1142	1.6	2.96	2.1	.1140	2.0	5.307	2.9	.3377	2.1	.714
10—4.2	c	65	17	.27	1,917.1	34.3	1,909.3	30.0	1,882.2	22.0	1,852	33.5	.3464	.0072	2.89	1.8	.1161	1.2	2.90	1.8	.1133	1.9	5.384	2.6	.3447	1.8	.700
10—19.1	c	189	131	.71	2,186.1	39.2	2,263.9	33.3	2,437.7	20.4	2,586	23.1	.4037	.0085	2.37	1.7	.1742	1.4	2.38	1.7	.1729	1.4	10.031	2.2	.4208	1.7	.784
10—18.1	c	92	88	.98	2,578.8	58.8	2,601.6	44.5	2,639.2	21.1	2,668	15.1	.4919	.0136	2.01	2.1	.1817	.9	2.01	2.1	.1817	.9	12.453	2.3	.4972	2.1	.916
Sample 98ADb55B																											
55B—6.1	—	708	70	0.10	173.1	2.4	173.5	2.4	178.4	4.1	— —	— —	0.0272	0.0004	36.59	1.4	0.0527	1.8	36.66	1.4	0.0511	2.1	0.192	2.5	0.0273	1.4	0.555
55B—9.1	—	4,776	963	.21	297.3	3.5	297.6	3.5	302.3	3.4	— —	— —	.0472	.0006	21.16	1.2	.0534	.5	21.16	1.2	.0532	.5	0.347	1.3	.0472	1.2	.917
55B—15.1	—	3,269	711	.22	302.9	3.6	303.1	3.6	306.0	3.6	— —	— —	.0481	.0006	20.75	1.2	.0537	.6	20.77	1.2	.0530	.6	0.352	1.4	.0481	1.2	.882
55B—19.1	—	2,308	470	.21	302.2	3.7	303.2	3.6	316.1	4.8	— —	— —	.0480	.0006	20.72	1.2	.0568	.7	20.77	1.2	.0550	1.3	0.365	1.8	.0482	1.2	.687
55B—14.1	—	1,411	307	.23	307.0	4.0	307.0	4.0	306.1	4.7	— —	— —	.0488	.0006	20.47	1.3	.0535	.8	20.50	1.3	.0523	1.2	0.352	1.8	.0488	1.3	.740

Table 1. U-Pb geochronologic data for (meta)igneous rocks of the West Point Complex and Salcha River gneiss dome—Continued

Spot name	Spot position	U (ppm)	Th (ppm)	$^{232}Th/^{238}U$ ratio	^{207}Pb-cr/$^{206}Pb/^{238}U$ age	1σ	^{204}Pb-cr/$^{206}Pb/^{238}U$ age	1σ	^{204}Pb-cr/$^{207}Pb/^{235}U$ age	1σ	^{204}Pb-cr/$^{207}Pb/^{206}Pb$ age	1σ	^{207}Pb-cr/^{206}Pb-r/^{238}U ratio	1σ	Total $^{238}U/^{206}Pb$ ratio	1σ	Total $^{207}Pb/^{206}Pb$ ratio	Error (pct)	^{204}Pb-cr/$^{238}U/^{206}Pb$-r	Error (pct)	^{204}Pb-cr/^{207}Pb-r/^{206}Pb-r	Error (pct)	^{204}Pb-cr/^{207}Pb-r/^{235}U	Error (pct)	^{204}Pb-cr/^{206}Pb-r/^{238}U	Error (pct)	err corr
Sample 98ADb55B																											
55B—5.1	—	935	203	.22	312.6	3.9	313.0	3.8	318.1	5.9	— —	— —	.0497	.0006	20.04	1.3	.0561	1.0	20.10	1.3	.0536	1.8	0.368	2.2	.0498	1.3	.576
55B—12.1	—	2,307	651	.29	321.9	3.9	322.3	3.9	327.3	4.1	— —	— —	.0512	.0006	19.50	1.2	.0538	.8	19.50	1.2	.0538	.8	0.380	1.5	.0513	1.2	.838
55B—13.1	—	1,779	333	.19	328.1	4.1	328.3	4.1	330.8	4.1	— —	— —	.0522	.0007	19.13	1.3	.0538	.6	19.14	1.3	.0535	.7	0.385	1.5	.0522	1.3	.874
55B—16.1	—	2,900	550	.20	331.0	4.3	331.1	4.3	333.1	4.5	— —	— —	.0527	.0007	18.96	1.3	.0538	.8	18.97	1.3	.0534	.9	0.388	1.6	.0527	1.3	.821
55B—11.1	—	1,451	347	.25	333.8	4.1	333.6	4.0	331.7	4.9	— —	— —	.0531	.0007	18.80	1.2	.0540	.9	18.83	1.2	.0528	1.2	0.386	1.7	.0531	1.2	.712
55B—8.1	—	1,161	346	.31	338.1	4.2	337.9	4.1	335.5	4.8	— —	— —	.0539	.0007	18.57	1.2	.0533	1.0	18.58	1.2	.0528	1.1	0.392	1.7	.0538	1.2	.747
55B—17.1	—	770	111	.15	339.4	4.2	339.1	4.1	334.9	5.0	— —	— —	.0541	.0007	18.50	1.3	.0533	1.0	18.52	1.3	.0525	1.2	0.391	1.8	.0540	1.3	.713
55B—18.1	—	2,269	612	.28	344.1	4.1	344.1	4.1	344.4	4.0	— —	— —	.0548	.0007	18.24	1.2	.0534	.6	18.24	1.2	.0534	.6	0.404	1.4	.0548	1.2	.886
55B—7.1	—	706	254	.37	350.2	4.4	350.5	4.4	353.7	5.3	— —	— —	.0558	.0007	17.90	1.3	.0541	1.2	17.90	1.3	.0541	1.2	0.417	1.8	.0559	1.3	.717
55B—1.1	—	453	96	.22	353.4	4.6	352.7	4.5	343.8	9.5	— —	— —	.0563	.0007	17.72	1.3	.0546	1.5	17.78	1.3	.0520	3.0	0.403	3.3	.0562	1.3	.405
55B—20.1	—	206	221	1.11	353.4	5.1	354.1	5.0	363.2	8.3	— —	— —	.0563	.0008	17.72	1.5	.0546	2.2	17.71	1.5	.0552	2.3	0.430	2.7	.0565	1.5	.534
55B—3.1	—	586	218	.38	355.1	4.5	355.2	4.5	355.9	5.6	— —	— —	.0566	.0007	17.65	1.3	.0538	1.4	17.65	1.3	.0538	1.4	0.420	1.9	.0566	1.3	.690
55B—10.1	—	1,224	423	.36	357.2	4.3	356.9	4.3	352.9	4.4	— —	— —	.0570	.0007	17.55	1.2	.0538	.8	17.57	1.2	.0530	.8	0.416	1.5	.0569	1.2	.823
55B—4.1	—	385	213	.57	363.1	4.8	362.5	4.7	354.5	7.2	— —	— —	.0579	.0008	17.25	1.3	.0539	1.6	17.29	1.3	.0524	2.0	0.418	2.4	.0578	1.3	.556
55B—2.1	—	2,740	732	.28	369.9	4.4	369.7	4.4	367.5	4.2	— —	— —	.0591	.0007	16.94	1.2	.0538	.6	16.94	1.2	.0536	.6	0.436	1.4	.0590	1.2	.897
Sample 98ADb66B																											
66B–26.1	c	919	94	0.11	78.8	1.6	78.8	1.6	79.7	3.8	– –	– –	0.0123	0.0003	80.95	2.0	0.0514	3.0	81.29	2.0	0.0482	4.6	0.082	5.0	0.0123	2.0	0.409
66B–12.2	r	1,402	171	.13	95.6	1.8	95.6	1.8	94.6	3.3	– –	– –	.0149	.0003	66.71	1.9	.0505	1.8	66.97	1.9	.0474	3.2	.098	3.7	.0149	1.9	.517
66B–30.1	r	757	76	.10	95.2	1.9	95.7	1.9	103.8	3.5	– –	– –	.0149	.0003	66.73	2.0	.0539	2.4	66.87	2.0	.0522	2.9	.108	3.5	.0150	2.0	.568
66B–8.2	r	5,043	172	.04	99.9	1.8	99.8	1.8	97.9	2.0	– –	– –	.0156	.0003	64.03	1.8	.0479	.9	64.10	1.8	.0470	1.1	.101	2.1	.0156	1.8	.854
66B–12.1	c	1,307	58	.05	100.5	1.9	100.6	1.9	103.0	2.6	– –	– –	.0157	.0003	63.56	1.9	.0492	1.9	63.56	1.9	.0492	1.9	.107	2.7	.0157	1.9	.712
66B–16.1	r	588	20	.04	101.9	2.1	101.8	2.1	100.6	3.2	– –	– –	.0159	.0003	62.82	2.0	.0474	2.7	62.82	2.0	.0474	2.7	.104	3.4	.0159	2.0	.600
66B–22.1	c	495	47	.10	107.0	2.2	106.6	2.1	99.9	6.0	– –	– –	.0167	.0003	59.62	2.0	.0500	4.9	60.00	2.0	.0450	6.0	.103	6.3	.0167	2.0	.318
66B–13.1	c	465	46	.10	108.7	2.2	108.3	2.2	102.7	4.5	– –	– –	.0170	.0003	58.83	2.0	.0482	3.0	59.03	2.0	.0456	4.2	.106	4.6	.0169	2.0	.438
66B–17.1	r	3,926	158	.04	112.2	2.0	112.2	2.0	112.1	2.2	– –	– –	.0176	.0003	56.94	1.8	.0482	1.0	56.94	1.8	.0482	1.0	.117	2.1	.0176	1.8	.880
66B–2.1	r	2,418	96	.04	112.4	2.1	112.5	2.0	114.3	2.5	– –	– –	.0176	.0003	56.74	1.8	.0500	1.2	56.80	1.8	.0491	1.4	.119	2.3	.0176	1.8	.786
66B–15.1	c	755	95	.13	112.7	2.2	112.5	2.2	109.7	3.9	– –	– –	.0176	.0003	56.79	1.9	.0470	3.2	56.79	1.9	.0470	3.2	.114	3.8	.0176	1.9	.517
66B–18.1	c	314	49	.16	113.4	2.4	113.4	2.4	112.7	6.4	– –	– –	.0178	.0004	55.97	2.1	.0533	3.3	56.35	2.1	.0480	5.6	.117	6.0	.0177	2.1	.352
66B–20.1	c	811	89	.11	114.4	2.2	114.6	2.2	118.5	3.2	– –	– –	.0179	.0003	55.74	1.9	.0500	2.2	55.74	1.9	.0500	2.2	.124	2.9	.0179	1.9	.663
66B–22.2	r	3,274	124	.04	114.8	2.1	114.7	2.1	112.5	3.6	– –	– –	.0180	.0003	55.36	1.8	.0523	1.4	55.70	1.8	.0473	2.8	.117	3.4	.0180	1.8	.545
66B–5.1	r	508	50	.10	115.5	2.3	115.5	2.3	116.4	3.6	– –	– –	.0181	.0004	55.30	2.0	.0487	2.7	55.30	2.0	.0487	2.7	.122	3.3	.0181	2.0	.600
66B–7.1	r	3,528	121	.04	118.9	2.2	118.8	2.2	117.3	3.7	– –	– –	.0186	.0003	53.36	1.8	.0534	1.5	53.75	1.8	.0477	2.7	.122	3.3	.0186	1.8	.556
66B–23.1	c	631	38	.06	119.0	2.3	119.1	2.3	121.4	5.0	– –	– –	.0186	.0004	53.43	2.0	.0521	2.4	53.61	2.0	.0494	3.9	.127	4.4	.0187	2.0	.447
66B–20.2	r	992	125	.13	119.2	2.3	119.5	2.3	123.6	3.2	– –	– –	.0187	.0004	53.47	1.9	.0502	1.9	53.47	1.9	.0502	1.9	.129	2.7	.0187	1.9	.701
66B–24.2	r	1,910	37	.02	120.1	2.3	120.2	2.3	121.7	9.2	– –	– –	.0188	.0004	52.05	1.9	.0653	2.2	53.13	1.9	.0491	7.8	.127	8.0	.0188	1.9	.241
66B–11B	r	1,141	153	.14	120.0	2.6	120.4	2.8	126.7	29.9	– –	– –	.0188	.0004	48.53	1.9	.1184	5.9	53.03	2.3	.0511	25.4	.133	25.5	.0189	2.3	.092
66B–1.1	r	6,867	166	.03	122.2	2.2	122.2	2.2	120.9	3.1	– –	– –	.0191	– –	51.83	1.8	.0546	1.1	52.28	1.8	.0479	2.1	.126	2.8	.0191	1.8	.656
66B–11	r	1,175	157	.14	120.9	6.9	119.9	8.1	– –	– –	– –	– –	.0189	.0011	39.27	2.9	.2525	11.5	53.27	6.8	– –	– –	– –	– –	.0188	6.8	– –
66B–10.1	r	613	75	.13	125.6	2.5	125.1	2.4	117.1	4.3	– –	– –	.0197	.0004	50.92	2.0	.0472	2.6	51.04	2.0	.0453	3.3	.122	3.9	.0196	2.0	.507
66B–3.1	c	88	1	.01	120.2	6.5	106.5	23.7	– –	– –	– –	– –	.0188	.0010	14.50	2.1	.6271	1.3	60.02	22.5	– –	– –	– –	– –	.0167	22.5	– –
66B–9.1	r	1,372	110	.08	138.9	2.6	139.6	2.6	150.3	3.8	– –	– –	.0218	.0004	45.60	1.9	.0541	1.7	45.67	1.9	.0529	1.9	.160	2.7	.0219	1.9	.701
66B–19.2	r	20,048	579	.03	170.6	3.0	170.9	3.0	174.8	3.0	– –	– –	.0268	.0005	37.20	1.8	.0513	.3	37.23	1.8	.0507	.4	.188	1.8	.0269	1.8	.976
66B–29.2	r	8,264	2,948	.37	223.7	4.3	223.8	5.9	224.4	63.2	– –	– –	.0353	.0007	19.94	1.8	.2874	.7	28.31	2.7	.0508	32.3	.247	32.4	.0353	2.7	.082
66B–6.1	c	358	312	.90	307.2	6.1	303.6	6.3	254.9	41.7	– –	– –	.0488	.0010	19.65	1.9	.0853	4.8	20.73	2.1	.0429	18.8	.285	18.9	.0482	2.1	.112
66B–28.1	c	4,875	1,234	.26	306.0	5.8	306.2	5.8	309.3	5.4	– –	– –	.0486	.0009	20.54	1.9	.0537	.5	20.56	1.9	.0531	0.6	.356	2.0	.0486	1.9	.950
66B–29.1	c	917	192	.22	357.4	6.8	357.0	6.7	352.1	12.2	– –	– –	.0570	.0011	17.40	1.9	.0601	1.8	17.56	1.9	.0528	3.7	.415	4.1	.0569	1.9	.467
66B–14.1	c	612	173	.29	601.9	11.4	627.1	13.4	858.9	63.2	– –	– –	.0979	.0019	9.19	1.9	.1423	2.5	9.79	2.2	.0944	11.0	1.330	11.2	.1022	2.2	.200
66B–24.1	c	236	30	.13	651.4	12.5	659.4	12.4	737.4	14.8	982	41.9	.1063	.0021	9.27	2.0	.0730	1.9	9.28	2.0	.0719	2.1	1.067	2.8	.1077	2.0	.692
66B–4.1	c	96	25	.26	827.5	16.3	829.2	15.8	844.1	15.8	884	39.1	.1370	.0029	7.29	2.0	.0685	1.9	7.29	2.0	.0685	1.9	1.296	2.8	.1373	2.0	.732
66B–8.1	c	686	191	.29	936.1	16.5	949.9	16.1	1,054.0	12.6	1,276	12.6	.1563	.0030	6.30	1.8	.0837	.6	6.30	1.8	.0833	.6	1.824	1.9	.1588	1.8	.943
66B–7.2	c	96	63	.69	1,057.5	20.5	1,059.4	19.6	1,073.3	17.9	1,102	36.7	.1783	.0038	5.59	2.0	.0779	1.6	5.60	2.0	.0762	1.8	1.878	2.7	.1786	2.0	.739
66B–9.1	c	50	26	.55	1,323.0	28.3	1,315.7	26.3	1,272.2	24.3	1,199	50.5	.2278	.0054	4.40	2.2	.0823	2.1	4.42	2.2	.0801	2.6	2.501	3.4	.2264	2.2	.653
66B–19.1	c	208	134	.66	1,598.6	29.3	1,643.3	27.3	1,822.0	17.4	2,033	15.6	.2814	.0058	3.44	1.9	.1253	.9	3.44	1.9	.1253	.9	5.016	2.1	.2904	1.9	.906
66B–25.1	c	292	137	.48	2,149.6	43.5	2,124.8	36.2	2,053.6	18.3	1,983	11.1	.3958	.0094	2.56	2.0	.1218	.6	2.56	2.0	.1218	.6	6.557	2.1	.3904	2.0	.955
66B–21.1	c	260	267	1.06	2,295.7	44.5	2,313.0	36.5	2,352.2	17.9	2,386	10.1	.4278	.0099	2.32	1.9	.1536	.6	2.32	1.9	.1536	.6	9.141	2.0	.4316	1.9	.953
66B–27.1	c	40	32	.84	2,662.9	65.7	2,661.7	47.9	2,659.8	23.2	2,658	19.5	.5115	.0154	1.95	2.2	.1825	1.1	1.96	2.2	.1806	1.2	12.729	2.5	.5112	2.2	.882

Table 2. $^{40}Ar/^{39}Ar$ single-grain laser step-heating data for biotite and white mica from sample 96ADb10A of West Point orthogneiss (see fig. 7).

[Weighted average of J (irradiation parameter) from standards: biotite, 0.009587±0.000038; white mica, 0.009205±0.000056]

Laser power (mW)	Cumulative ^{39}Ar	$^{40}Ar/^{39}Ar$ ratio	1σ	$^{37}Ar/^{39}Ar$ ratio	1σ	$^{36}Ar/^{39}Ar$ ratio	1σ	Atm. ^{40}Ar (pct)	Ca/K ratio	1σ	Cl/K ratio	1σ	Radiogenic $^{40}Ar/^{39}K$ ratio	1σ	Age (Ma)	1σ (Ma)
96ADb10A (biotite)																
100	0.012	6.415	0.029	0.0340	0.0051	0.01089	0.00085	50.4	0.0624	0.0094	0.00290	0.00017	3.170	0.253	54.0	4.2
150	.059	5.891	.012	.0098	.0011	.00228	.00022	11.5	.0180	.0021	.00356	.00005	5.189	.065	87.6	1.1
200	.174	5.437	.011	.0012	.0004	.00056	.00008	3.0	.0021	.0008	.00365	.00003	5.244	.025	88.5	.4
300	.331	5.288	.016	.0017	.0004	—.00004	.00005	—.2	.0032	.0007	.00362	.00006	5.270	.022	88.9	.4
450	.506	5.287	.021	.0032	.0003	—.00014	.00004	—.8	.0059	.0005	.00350	.00006	5.299	.024	89.4	.4
600	.711	5.307	.017	.0021	.0003	.00002	.00003	.1	.0039	.0005	.00377	.00006	5.273	.020	89.0	.3
750	.850	5.228	.022	.0021	.0006	—.00020	.00005	—1.2	.0039	.0010	.00383	.00006	5.260	.027	88.8	.5
900	.920	5.273	.023	.0079	.0009	—.00027	.00010	—1.5	.0145	.0017	.00376	.00006	5.325	.038	89.8	.6
1,100	.933	5.166	.055	.0483	.0051	—.00078	.00064	—4.6	.0886	.0094	.00349	.00020	5.373	.198	90.6	3.3
1,300	.945	5.108	.048	.0955	.0055	—.00138	.00050	—8.2	.1752	.0102	.00371	.00027	5.495	.155	92.6	2.6
1,500	.955	5.008	.073	.0226	.0054	—.00169	.00087	—10.1	.0415	.0100	.00400	.00032	5.480	.267	92.4	4.4
1,750	.965	4.984	.057	.1308	.0055	—.00299	.00046	—18.1	.2401	.0101	.00390	.00033	5.851	.149	98.5	2.4
2,000	.982	5.189	.057	.0471	.0038	—.00103	.00032	—6.0	.0863	.0070	.00370	.00015	5.469	.113	92.2	1.9
3,000	.995	4.997	.042	—.0019	.0041	—.00292	.00043	—17.4	—.0036	.0076	.00326	.00018	5.831	.135	98.1	2.2
8,000	1.000	4.663	.053	.0004	.0116	—.00473	.00088	—30.2	.0007	.0214	.00411	.00053	6.032	.268	101.4	4.4
Integrated----------		5.323	.007	.0072	.0002	.00007	.00003	.4	.0132	.0004	.00367	.00002	5.273	.011	89.0	.4
96ADb10A (white mica)																
300	0.006	6.143	0.022	0.0101	0.0023	0.00151	0.00045	7.3	0.0186	0.0042	0.00026	0.00020	5.669	0.135	91.8	2.1
400	.008	6.988	.081	.0143	.0095	.00189	.00131	8.0	.0263	.0175	.00083	.00049	6.401	.394	103.3	6.2
600	.020	6.100	.022	.0109	.0012	.00171	.00019	8.3	.0200	.0021	.00056	.00010	5.567	.061	90.2	1.0
800	.047	6.284	.006	.0044	.0006	.00121	.00012	5.7	.0081	.0011	.00041	.00003	5.898	.035	95.4	.6
1,000	.089	6.432	.009	.0012	.0003	.00190	.00008	8.8	.0022	.0005	.00046	.00006	5.842	.025	94.5	.4
1,200	.148	6.340	.012	.0017	.0003	.00103	.00007	4.8	.0031	.0006	.00038	.00002	6.008	.024	97.1	.4
1,400	.258	6.272	.010	.0018	.0002	.00111	.00003	5.2	.0033	.0004	.00040	.00002	5.916	.013	95.7	.2
1,700	.372	6.298	.011	.0013	.0002	.00110	.00005	5.2	.0023	.0004	.00036	.00002	5.944	.019	96.1	.3
2,000	.511	6.217	.024	.0023	.0001	.00081	.00003	3.9	.0042	.0003	.00046	.00002	5.948	.025	96.2	.4
3,000	.725	6.153	.022	.0027	.0001	.00095	.00002	4.6	.0050	.0002	.00041	.00003	5.844	.023	94.5	.4
4,000	.810	6.228	.011	.0007	.0002	.00057	.00007	2.7	.0013	.0003	.00040	.00003	6.031	.023	97.5	.4
7,000	.982	6.295	.021	.0010	.0001	.00078	.00001	3.7	.0018	.0002	.00038	.00002	6.037	.021	97.6	.3
8,000	1.000	6.311	.022	.1388	.0015	.00124	.00014	5.7	.2547	.0028	.00054	.00008	5.927	.047	95.8	.7
Integrated----------		6.252	.007	.0044	.0001	.00097	.00001	4.6	.0081	.0001	.00041	.00001	5.936	.008	96.0	.6

margin of the Salcha River gneiss dome (fig. 2); we interpret this dike to be part of an undeformed stock that intrudes the dome. A conventional U-Pb zircon age of 116±3 Ma was previously determined for a granitoid sample from that stock (fig. 2; Aleinikoff and others, 1984a).

U-Pb Zircon Data

Analytical Techniques

U-Pb zircon analyses were conducted on the SHRIMP–RG (reverse geometry) ion microprobe co-operated by the U.S. Geological Survey (USGS) and Stanford University. Zircons, concentrated by standard heavy-mineral-separation processes, were mounted in epoxy, polished, and imaged with transmitted light, reflected light, and cathodoluminescence to identify internal structures and defects. The mounted zircons were washed with 1 *N* HCl and distilled water, dried, and coated with approximately 10 nm of Au. The primary O_2^- ion beam (~8–15 nA) typically produces a spot with a diameter of 30 to 40 µm and a depth of 1 to 2 µm for an analysis time of 9–12 minutes. Concentration data were standardized against zircon standard SL–13 (238 ppm U) and are accurate to about 10 to 20 percent, and age data were standardized against zircons AS3 and AS57 (1,098 Ma from the anorthositic gabbro, Duluth Complex; Paces and Miller, 1993), which were analyzed repeatedly throughout the duration of the session. Data reduction followed the method of Williams (1998), using the PRAWN and LEAD program of T.R. Ireland (unpub. program routine) and the Squid and Isoplot/Ex program of Ludwig (2001).

U-Pb data are generally plotted on either a Tera-Wasserburg or a Wetherill concordia diagram. Tera-Wasserburg concordia diagrams are plotted with data uncorrected for common Pb because only these data allow the determination of age trends that may result from mixing of zircons of different ages or from loss of radiogenic Pb, whereas a Wetherill concordia diagram is plotted with data corrected for the measured ^{204}Pb content in each spot. Because most Phanerozoic zircons contain only traces of ^{207}Pb and ion-microprobe analyses consume only 1 to 2 ng of material, counting statistics for ^{207}Pb are poor, and atomic ratios involving ^{207}Pb, especially the $^{207}Pb/^{235}U$ ratio needed for Wetherill concordia diagrams, have relatively high analytical uncertainties. $^{207}Pb/^{206}Pb$ ratios, however, can be measured much more precisely than $^{204}Pb/^{206}Pb$ ratios, and so $^{206}Pb/^{238}U$ ages corrected by using measured $^{207}Pb/^{206}Pb$ ratios are most reliable for ion-microprobe data from Phanerozoic samples, whereas a Tera-Wasserburg concordia diagram is preferred for evaluating and displaying these data.

Results

Sample 96ADb10A

Ion-microprobe spot analyses of sample 96ADb10A (table 1) were made for 33 zircon grains separated from the West Point orthogneiss. In transmitted light, the zircons are mostly subhedral, elongate, doubly terminated prisms, with lesser amounts of anhedral crystals and broken grains (fig. 4). In scanning-electron-microscope cathodoluminescence (SEM–CL) images (fig. 4*C*, 4*D*, and 4*E*), grain interiors are generally dark (that is, U rich) and exhibit euhedral oscillatory zoning, commonly surrounded by a light (that is, U poor) outer margin that, in turn, is overgrown by a medium-gray rim, which in some zircons contains concentrically arranged oscillatory zoning. Ion-microprobe spot analyses of zircon cores, homogeneous grains, and rims clearly indicate that the previous multigrain TIMS age for this sample (671±34 Ma; Smith and others, 1994), which Smith and others interpreted as the time of igneous crystallization of the granitic orthogneiss, actually averaged several distinct isotopic populations. U-Pb ion-microprobe spot analyses within most cores, such as in grains 1 and 2 (figs. 4*C,* 4*D*), yield Devonian ages, but several other cores yielded Archean or Proterozoic ages of ~2.6, 1.8, 1.4, and 1.1 Ga (fig. 5*A*; table 1). In contrast, zircon rims on 13 out of 15 grains (such as those shown for grains 1 and 2) and one partial fragment of what might be a complete grain (grain 26, fig. 4*E*) yielded Early Cretaceous ages (table 1). A plot of $^{206}Pb/^{238}U$ age versus Th/U ratio for individual zircon spot analyses (fig. 6*A*) shows that the Th/U ratios are very low (<0.2) for the spots that yielded Early Cretaceous ages. These very low Th/U ratios generally indicate zircons grown under fluid-rich, oxidizing conditions—either in a metamorphic or a fluid-rich magmatic environment. In contrast, the variation in the Th/U ratio of Devonian (~375 Ma) zircon cores is typical of that of magmatic zircons.

The Tera-Wasserburg concordia diagram for this sample (fig. 5*A*) illustrates the systematics of the spots that yielded Phanerozoic ages. Four discordia lines (dashed lines, fig. 5*A*) are drawn through the data points to indicate possible interpretations of these data. Two of the chords (red ovals on left, fig. 5*A*) connect a large population of Devonian (~375±8 Ma) cores with older data for other zircon cores from this sample. The upper-intercept ages of these two discordia should not be taken specifically but only as an indication of Late Archean and Protoproterozoic ages that we interpret as the general inheritance ages from crustal materials. These ages (~2.6 and 1.8 Ga, respectively) are commonly observed as inheritance ages in felsic magmatic rocks (Aleinikoff and others, 1986; Heslop and others, 1995; Dusel-Bacon and Aleinikoff, 1996) and as detrital ages in metasedimentary rocks of the Yukon-Tanana Upland (Aleinikoff and others, 1984b, 1995; Foster and others, 1987). The other two discordia lines pass through the Early Cretaceous zircon population, one of which (green ovals, fig. 5*A*) connects the Early Cretaceous zircon population with the Devonian core ages, illustrating a possible mixing trend between the two populations and (or) an episodic Pb-loss trend for Devonian grains affected by Cretaceous events. A mixing trend would most likely result from placement of the ion-microprobe spot on the boundary between two ages of zircons. The ages for this discordia, particularly the younger age, are not meant to indicate the actual ages of specific geologic events. The other discordia line is defined by the seven grains (red ovals on right, fig. 5*A*) with the youngest Early

Cretaceous ages. The steep trend of this discordia line and its rightward slant indicate that these grains have undergone Pb loss. The lower-intercept age of this discordia line is the same, within error, as the weighted-mean-average age of 112±2 Ma for seven of the most concordant spots from zircon rims (spots 10–1.1 through 10–26.1, table 1). Eliminating from this group two grains with very high U contents, which may cause calibration problems (Williams and Hergt, 2000), gives an age of 111±2 Ma. Four spots (10–33.1 through 10–6.1, table 1) on rims with very high U contents (5,000–8,000 ppm) yielded ages of 121 to 129 Ma, which also may be unreliable because of calibration problems. The U-Pb systematics in this sample are clearly complex. Although the effects of the metamorphic event on this rock have not been accounted for in this interpretation, this event must have occurred 111 Ma or later if the crystallization age has been correctly identified.

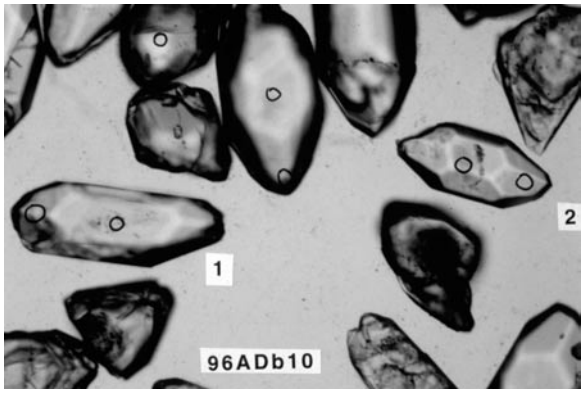

A

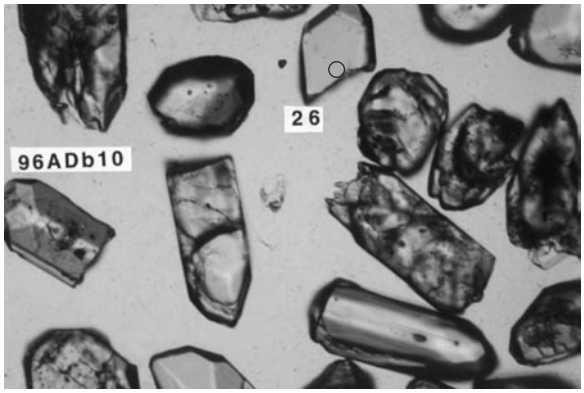

B

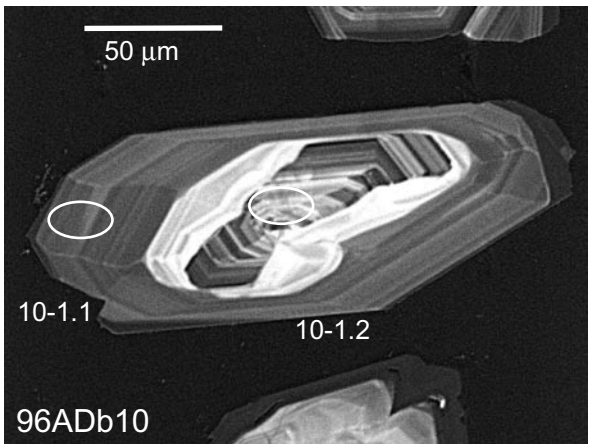

C

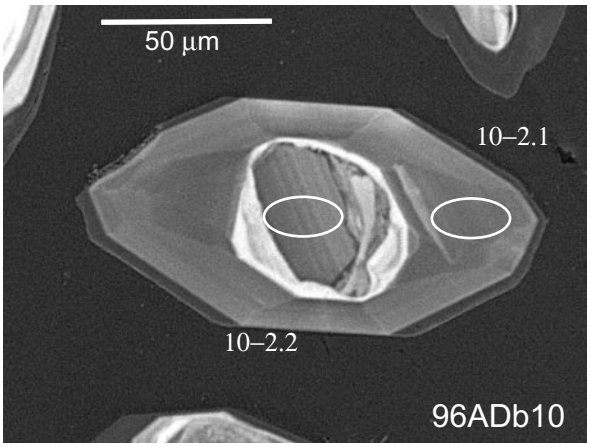

D

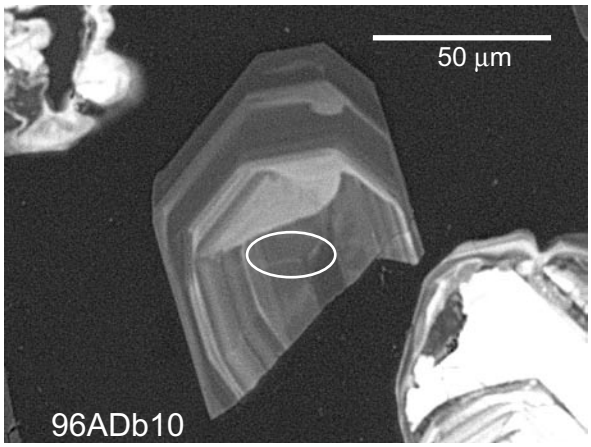

E

Figure 4. Photomicrographs of selected zircons separated from sample 96ADb10A of West Point orthogneiss (table 1). Numbers, analyzed grains; circles in figures 4*A*, 4*B*, locations of ion-microprobe spot analyses. Figures 4*A* and 4*B* were taken in transmitted light; figures 4*C* through 4*E* are scanning-electron-microscope cathodoluminescence images, in which ellipses show outlines of ion-microprobe analytical spots, approximately 20 μm in diameter and 2 μm deep.

Sample 98ADb55B

Zircons from sample 98ADb55B (tables 1, 4) are blocky, 100 to 200 µm long, with regular to irregular compositional zoning. Rim and core structures are not as obvious as in samples 96ADb10A (fig. 4; table 1) and 98ADb66B (table 1), although cores may be present. We made no attempt to find cores with the ion microprobe, because our primary objective was to determine the crystallization age. However, augen gneiss samples containing zircons without obvious inheritance is unusual for the Lake George assemblage. The 20 analyses on this sample concentrated on the edges of grains and provided an age range from 173 to 370 Ma (fig. 5*B*; table 1). Although most of the older ages plot on or near concordia, a clear trend away from concordia defines a discordia line with an upper-intercept age of 360±13 Ma and a lower-intercept age of 44±69 Ma. U contents range from 200 to almost 5,000 ppm in these spots, and the younger ages are approximately associated with higher U contents. This correlation supports the interpretation of this discordia line as reflecting Pb loss. Although the lower-intercept age is too imprecise to be meaningful, the upper-intercept age provides a general estimate of the crystallization age. Six spots (55B–7.1 through 55B–4.1, table 1), all with lower U contents, yielded a weighted-mean-average age of 355±4 Ma, which is probably the best estimate of the crystallization age of this sample. We interpret these data to indicate a crystallization age of about 355 Ma for the protolith of the augen gneiss and to suggest an episodic event(s) during the mid-Cretaceous and (or) Tertiary that disturbed the U-Pb systematics of these zircons. Possible causes of Pb loss include mid-Cretaceous plutonism (that we interpret to have formed the West Point orthogneiss), mid-Cretaceous crustal extension (Pavlis and others, 1993), latest Cretaceous and early Tertiary plutonism (Wilson and others, 1985; Smith and others, 1994), and Eocene uplift, as suggested by apatite fission-track ages (Dusel-Bacon and Murphy, 2001).

Sample 98ADb66B

Sample 98ADb66B (tables 1, 4) is an undeformed granitoid that we interpret to be a dike. The zircons generally range in length from 100 to 200 µm, are subhedral to euhedral with double terminations, and many grains have conspicuous high-U rims and lower-U cores. U-Pb ages range from 79 to 2,600 Ma; all ages older than 300 Ma were found in cores (fig. 5*C*; table 1). Older core ages are mostly Precambrian, but even these ages range from about 827 to 2,700 Ma, with no age grouping. Zircons with ages of 96 to 126 Ma dominate the analyzed population. These ages were measured on both zircon rims and cores that have U contents ranging from 300 to almost 7,000 ppm. Th/U ratios for these younger zircons are all less than 0.2 and, as discussed for sample 96ADb10A (table 1), indicate a fluid-rich, oxidizing system. Unlike the West Point orthogneiss, however, this granitoid has no planar fabric and is clearly postkinematic;

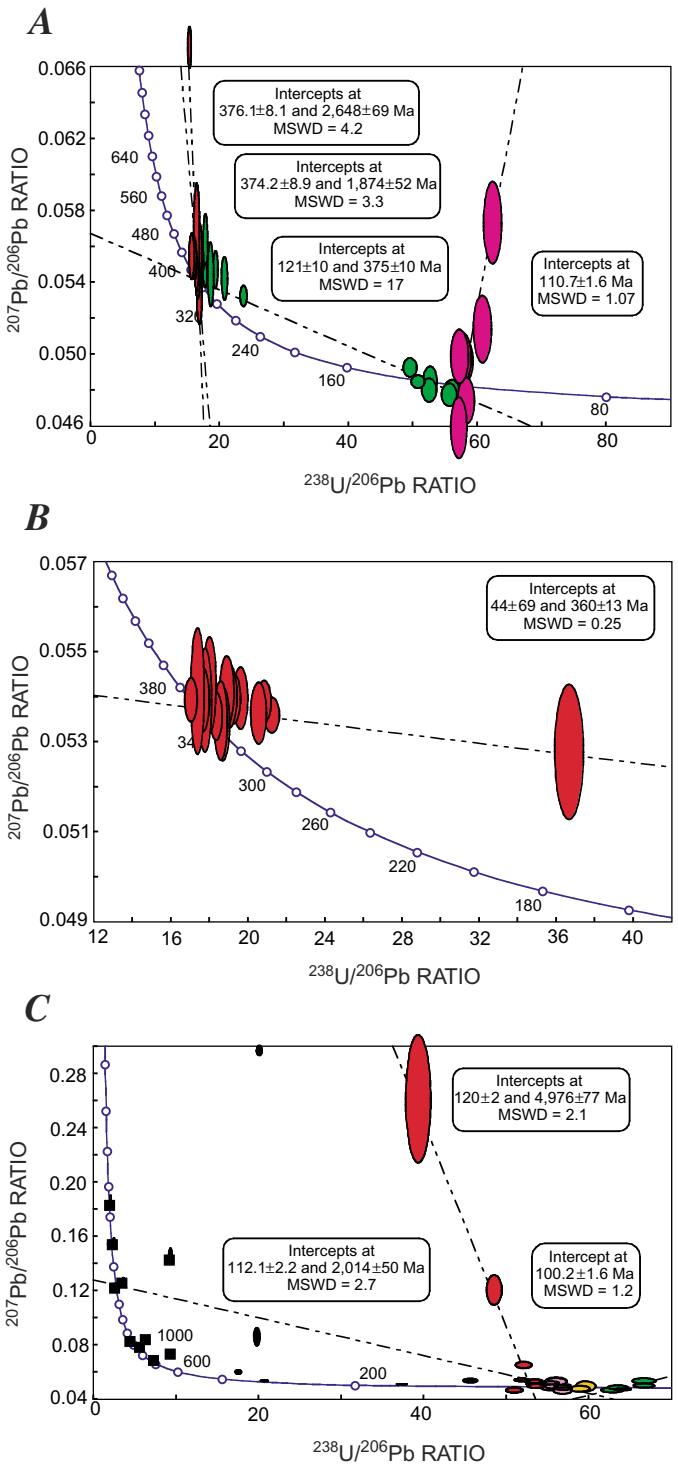

Figure 5. Tera-Wasserburg concordia plot for ion-microprobe U-Pb zircon samples 96ADb10A (*A*), 98ADb55B (*B*), and 98ADb66B (*C*) (table 1). See text for explanation of colored error ellipses. In figure 5*C*, black error ellipses and squares (substituted for error ellipses that are too small to be easily distinguished on plot) show data points that were omitted from interpretation of Cretaceous crystallization age for this sample. MSWD, mean standard of weighted deviates.

thus, its Early Cretaceous crystallization was magmatic, not metamorphic. Although the sample must have an Early Cretaceous age of 100 to 120 Ma, the U-Pb systematics of these younger spot analyses are highly complex, and an unambiguous age cannot easily be determined for the igneous-crystallization event. In the following discussion, we ignore any possible calibration problems that might have resulted from high U contents because no obvious pattern of U contents is apparent in this data set.

Three discordia lines are used to illustrate possible age trends in the Cretaceous grains. Nine spots (66B–7.1 through 66B–3.1, table 1) on seven rims and two cores (red ellipses, fig. 5*C*) define a discordia line with a lower-intercept age of 120±2 Ma and an upper-intercept age of 4,976±77 Ma. This age trend clearly results from some grains (four with strongly discordant data) incorporating significant amounts of common Pb during their formation. Although the upper-intercept age of this trend is not geologically significant, the lower-intercept age provides a good estimate of the maximum crystallization age. The second discordia line, with lower- and upper-intercept ages of 112±2 and 2,014±50 Ma, respectively, is provided only as an example of a mixing trend between Cretaceous and older inherited cores and (or) of Cretaceous episodic Pb loss from older cores. The mixing and (or) episodic Pb loss do not seem to have been important factors in our interpretation of the Cretaceous U-Pb data. The third discordia line, defined by five spots (66B–12.2 through 66B–16.1, table 1) on four rims and one core (green ellipses, fig. 5*C*), intersects the concordia at 100.2±1.6 Ma, suggesting a recent Pb-loss trend nearly identical to that observed in sample 96ADb10A. This intercept, which is clearly a minimum crystallization age, more likely represents a group of grains strongly affected by Pb loss. Some analyses (yellow ellipses, fig. 5*C*) were excluded from age calculations because they probably represent partial Pb loss. Seven concordant spots (66B–17.1 through 66B–51, table 1) on three cores and five rims (pink ellipses, fig. 5*C*) provide a weighted-mean-average age of 113±2 Ma that could represent the crystallization age, because these grains appear to be unaffected by Pb loss. Although the weighted-mean-average age of 14 spots with ages ranging from 107 to 122 Ma is 114±3 Ma, this suite clearly seems to include spots from at least two groups with average ages of about 113 and 120 Ma. We are unable to decide whether 113 or 120 Ma is the best estimate of the crystallization age, but we prefer the 113±2-Ma age because it is not complicated by any significant common-Pb component or by evidence of Pb loss.

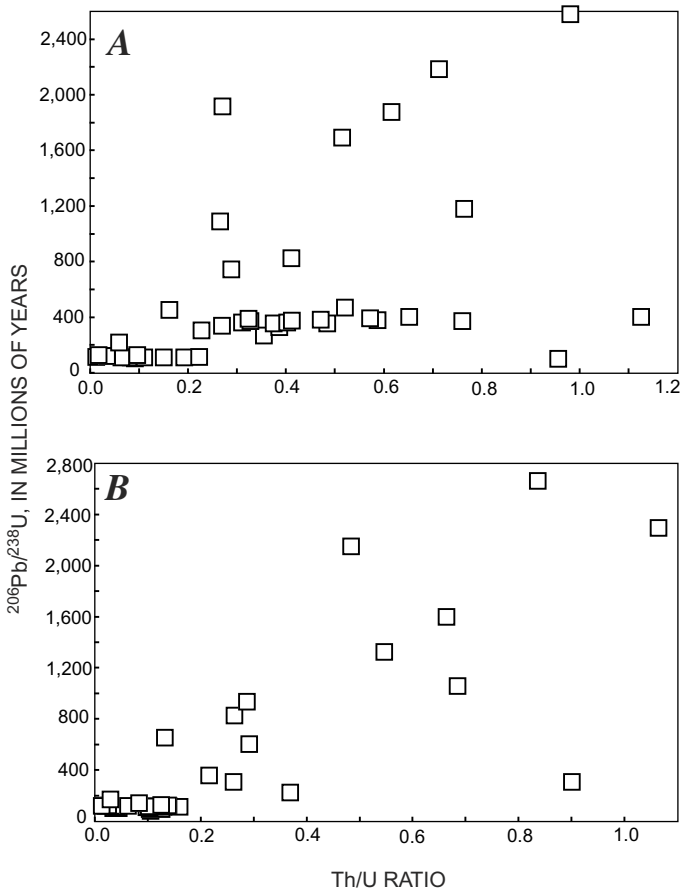

Figure 6. $^{206}Pb/^{238}U$ age versus Th/U ratio for spot analyses of individual zircons in samples 96ADb10A (*A*) and 98ADb66B (*B*) (table 1).

Interpretation of U-Pb data

As mentioned above, the Early Cretaceous (111±2 Ma) U-Pb ages for zircon rims from the West Point orthogneiss could represent either magmatic or metamorphic crystallization of new zircon. In magmatic crystallization, Early Cretaceous zircon rims (and one newly formed zircon) would have formed during a Cretaceous magmatic event in which wallrocks that included quartzite, pelitic schist, and Devonian augen gneiss were remobilized (anatectically melting); metamorphism of the gneiss would have followed shortly thereafter but not have resulted in the formation of new zircon rims. In metamorphic crystallization, the Early Cretaceous zircon rims would have formed during amphibolite-facies metamorphism of a Devonian intrusion. The morphology of zircons in the West Point orthogneiss and the conditions necessary to form metamorphic zircon are important factors that bear on our evaluation of these two possible events.

Accessory zircon typically forms as a liquidus phase in magmas of granitic to tonalitic composition (Poldervaart, 1956). Bipyramidal prisms with euhedral internal zoning and long needlelike inclusions are characteristic of unimpeded growth in a liquid (Silver, 1969). Metamorphic zircons grown in mafic igneous rocks under amphibolite-, granulite-, and eclogite-facies conditions are generally rounded to elongate, with small crystal faces, rounded edges, and patchy and irregular growth zones (see Creaser and others, 1997). Metamorphic mantles and rims around igneous zircons have been observed in pyroxene-bearing intrusions metamorphosed under both granulite-facies (van Breemen and others, 1986, 1987) and upper-amphibolite-facies (Barr and others, 1987) conditions. Metamorphic reactions involving breakdown of the high-Zr

phases orthopyroxene, clinopyroxene, and amphibole are the most likely sources for the zirconium in the metamorphic rims. The metamorphic zircon mantles observed by van Breemen and others (1986, 1987) and Barr and others (1987) generally do not conform to the inner morphology of the magmatic zircon cores.

The formation of metamorphic zircons and metamorphic rims on preexisting igneous zircon cores in granitic rocks devoid of pyroxene or amphibole is not so well established. A phenomenon called Ostwald ripening, in which large crystals tend to grow at the expense of smaller crystals so as to minimize their surface energy, appears to be a factor in the coarsening of grain size in high-grade, granulite-facies rocks (Spear, 1993). This same principle could apply to the formation of zircon rims derived from the redistribution of zircon from smaller crystals during high-grade metamorphism.

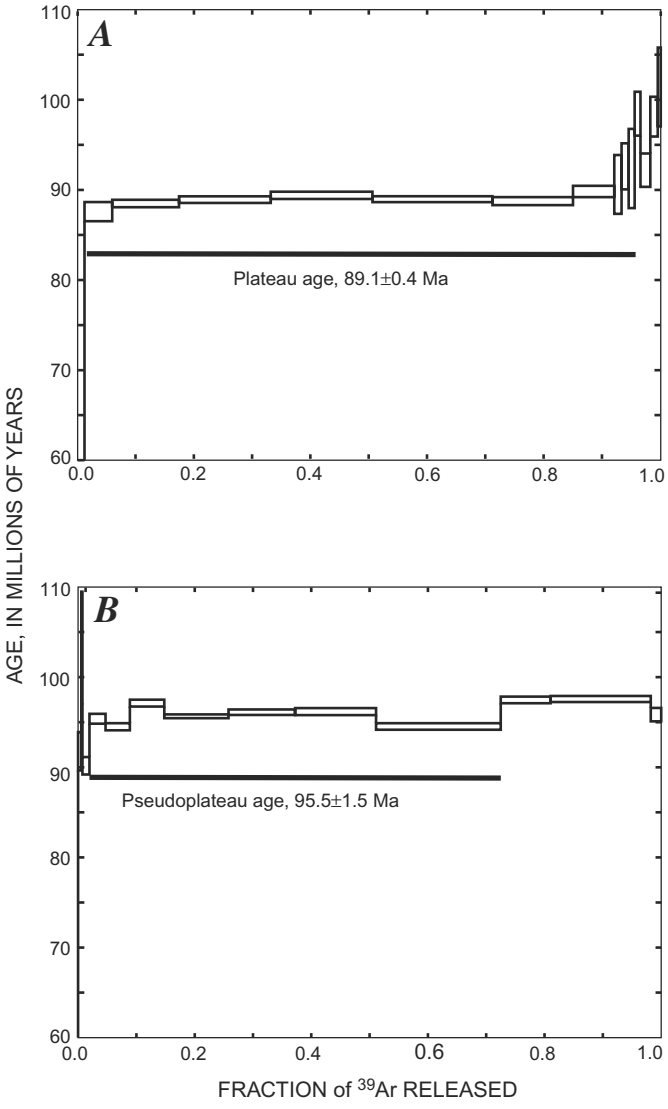

Figure 7. Ar-release spectra for biotite (*A*) and white mica (*B*) from sample 96ADb10A of West Point orthogneiss (tables 2, 3). Box heights of each rectangle are ±1σ.

Given the paucity of definitive studies involving the interpretation of mantles and rims on igneous zircons in granitic rocks that are devoid of pyroxene or amphibole, we conclude that it is impossible to unequivocally determine whether the zircon rims in the West Point orthogneiss formed under magmatic or metamorphic conditions. Nevertheless, we favor a magmatic origin for the zircon rims in the West Point orthogneiss for the following reasons. (1) Many zircon rims show features indicative of magmatic crystallization, including oscillatory growth zoning (clearly displayed at the margin of grain 1, fig. 4*C*, which yielded a 109.8-Ma age), the presence of needlelike inclusions (observed in the outer rims of a few zircon grains), and elongate and well-faceted terminations. (2) A previous U-Pb SHRIMP study of zircons from four different samples of augen gneiss from the Lake George assemblage in the eastern Yukon-Tanana Upland revealed no evidence for metamorphic rims on Devonian (~360 Ma) zircons (Heslop and others, 1995), in spite of the fact that wallrocks to the augen gneiss underwent high-pressure (7–12 kbars) and moderate- to high-temperature (500–700°C) metamorphism (Dusel-Bacon and others, 1995). We consider it unlikely that the metamorphic grade in the vicinity of the West Point orthogneiss (believed to be <650°C, as stated above) was high enough to cause any precipitation of new zircon. The mineralogy of the samples of granitoid orthogneiss in these two studies is similar.

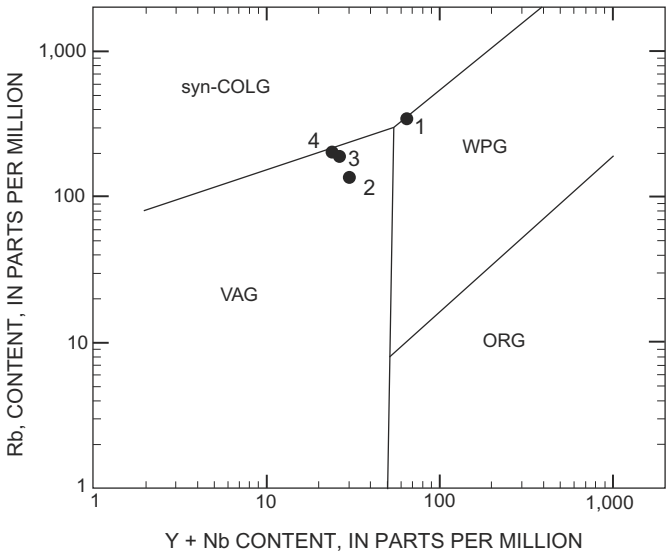

Figure 8. Rb–Y+Nb tectonic discrimination diagram (Pearce and others, 1984) for granitic samples from areas of West Point orthogneiss and Salcha River gneiss dome. Samples: 1, 98ADb55B, Devonian augen gneiss sample; 2, 98ADb53B, undated granitic orthogneiss from the West Point Complex; 3, 96ADb10A, Cretaceous granitic orthogneiss from the West Point Complex; 4, 98ADb66B, Cretaceous granitic dike that intrudes the Salcha River gneiss dome. See table 4 for complete geochemical analyses. ORG, orogenic granite; syn-COLG, syncollisional granite; VAG, volcanic-arc granite; WPG, within-plate granite.

Table 3. Summary of $^{40}Ar/^{39}Ar$ ages for biotite and white mica from sample 96ADb10A of West Point orthogneiss.

[Samples were run against standard Mmhb–1 (513.9 Ma) and processed by using the constants of Steiger and Jäger (1977). Bold ages, interpreted; error limits, 1σ. MSWD, mean standard of weighted deviates]

Mineral	Integrated age (Ma)	Plateau age (Ma)	Comments
Biotite--------	89.0±0.4	89.1±0.4	10-fraction plateau, 94-percent gas release; MSWD=1.0.
White mica---	96.0±0.6	95.5±1.5	7-fraction pseudoplateau, 71-percent gas release; MSWD=6.5.

In spite of our preferred crystallization age of 111±2 Ma for the West Point orthogneiss, we recognize that this interpretation is equivocal and still leaves open the exact temporal relation between intrusion of the gneiss protolith and subsequent metamorphism. A TIMS U-Pb age on monazite from the previously dated sample of West Point orthogneiss is 116±4 Ma (J.N. Aleinikoff, written commun., 2002). Thus, the monazite age and the zircon age agree within analytical uncertainty. The monazite could have crystallized either during intrusion of the granitoid or during subsequent regional metamorphism. Independent geologic evidence, discussed in the section below entitled "Tectonic Implications," indicates the near-contemporaneity of mid-Cretaceous metamorphism and posttectonic plutonism, and so ascribing either a metamorphic or an igneous origin to the zircon rims in the West Point orthogneiss is a somewhat academic question.

$^{40}Ar/^{39}Ar$ Data

Analytical Techniques

A sample of West Point orthogneiss (96ADb10A, tables 1–4) from the same locality at which the U-Pb sample was collected was submitted to the Geochronology Laboratory of the University of Alaska, Fairbanks, for $^{40}Ar/^{39}Ar$ analysis of the biotite and white mica. The mica separates were wrapped in aluminum foil and arranged in one of two levels, labeled top or bottom, within aluminum cans, 2.5 cm in diameter and 4.5 cm high. Samples were run against standard MMhb–1 (Samson and Alexander, 1987), dated at 513.9 Ma (Lanphere and others, 1990). The samples were irradiated at 35 MW-h in position 5C of the uranium-enriched research reactor of McMaster University in Hamilton, Ontario, Canada.

Upon their return from the reactor, the sample and monitors were loaded into 2-mm-diameter holes in a copper tray, which was then loaded in an ultra-high-vacuum extraction line. The monitors were fused, and the sample was step-heated, using a 6-W Ar-ion laser, according to the method of York and others (1981) and Layer and others (1987). Ar was purified by using a liquid nitrogen cold trap and an SAES Zr-Al getter at 400°C. The samples were then analyzed on a VG–3600 mass spectrometer at the Geophysical Institute of the University of Alaska, Fairbanks. The measured Ar isotopes were corrected for system blank and mass discrimination, as well as for Ca-, K-, and Cl-interference reactions, according to the method of McDougall and Harrison (1988).

$^{40}Ar/^{39}Ar$ Results

Detailed analyses are listed in table 2, and the $^{40}Ar/^{39}Ar$ results are summarized in table 3. The biotite analysis yields a flat age spectrum, with a plateau age of 89.0±0.4 Ma and an indication of a slight Ar loss at ~54 Ma. The spectra steps up to an older age of 101.4±4.4 Ma in the last 10 percent of gas release. This sample may have been originally older than the plateau age.

The sample of white mica was irradiated separately from the biotite above, and two splits of the separate were run. In the first run, the raw data were lost because of a hard-drive failure. Both spectra from this sample show a shallow U-shaped plateau and some Ar loss, with hints of excess Ar. The white mica is significantly older than the biotite. In the second run, the white mica yielded a pseudoplateau age of 95.5±1.5 Ma, consistent with visual inspection of the data from the first run and a calculated plateau age of 95.6±0.6 Ma based on the summary output data.

Interpretation of $^{40}Ar/^{39}Ar$ Data

The $^{40}Ar/^{39}Ar$ plateau age of 89 Ma for biotite from our sample of West Point orthogneiss overlaps a K-Ar age of 89.8±2.7 Ma that was determined for biotite from the previously dated U-Pb zircon sample whose upper-intercept age was interpreted by Smith and others (1994) to indicate a Late Proterozoic crystallization age for the orthogneiss. K-Ar ages for biotite and hornblende pairs from three different undeformed plutons in the study area to the southeast of West Point (fig. 1) fall in the range 92–96 Ma. In the study area north of West Point, a K-Ar age of 85 Ma was determined for biotite from the southernmost small pluton, and biotite and muscovite pairs gave K-Ar ages in the range 68–77 Ma for plutons farther to the north (Smith and others, 1994). In agreement with Smith and others, we interpret our biotite age as a thermal overprint from the numerous unmetamorphosed Cretaceous and Tertiary age plutons in the study area.

Table 4. Geochemical analyses of samples of granite and orthogneiss discussed in text.

[Quadrangles: BD, Big Delta; CI, Circle. Major- and minor-element-oxide contents in weight percent; trace-element contents in parts per million. Analyzed at the GeoAnalytical laboratory, Washington State University, Pullman. Trace-element contents of V, Cr, Ni, Cu, Zn, Ga, and Zr determined by wavelength-dispersive X-ray-fluorescence analysis and of other elements by inductively coupled plasma mass-spectrometric analysis. LOI, weight loss on ignition]

Sample	98ADb55B	98ADb53B	96ADb10A	98ADb66B
No. (fig. 8)	1	2	3	4
Rock type	Augen gneiss	Granite orthogneiss	Granite orthogneiss	Granitic dike intruding sillimanite gneiss
Lat, long	65°00′47″ N., 144°56′15″ W.	64°58′45″ N., 144°53′38″ W.	64°55′30″ N., 144°49′30″ W.	64°37′50″ N., 145°40′22″ W.
Quadrangle	CI A–2	BD D–2	BD D–2	BD C–4
Major- and minor-element oxides				
SiO_2	73.51	73.51	74.49	72.67
Al_2O_3	13.80	14.21	14.06	14.91
FeO	1.53	1.76	1.36	.59
MgO	.32	.36	.34	.19
CaO	.94	1.82	1.29	1.36
Na_2O	3.01	2.88	2.40	2.40
K_2O	6.14	4.17	5.50	7.14
TiO_2	.22	.14	.18	.07
P_2O_5	.06	.11	.07	.10
MnO	.03	.05	.02	.02
Total	99.56	99.00	99.71	99.44
LOI	.49	.91	.53	.40
Trace elements				
Sc	6.20	9.20	4.20	3.90
V	19	19	12	5
Cr	4	2	9	0
Ni	7	6	9	3
Cu	7	3	13	2
Zn	50	34	37	15
Ga	20	14	17	18
Rb	341	135	187	200
Cs	5.13	2.90	2.69	6.43
Sr	101	190	180	171
Ba	735	796	642	487
Pb	26.00	19.40	41.30	57.50
La	44.85	33.68	39.05	10.10
Ce	81.07	65.37	73.42	21.23
Pr	8.75	7.39	7.93	2.56
Nd	30.76	28.23	29.46	9.66
Sm	7.10	6.00	7.25	2.71
Eu	.57	1.22	1.02	.73
Gd	6.44	3.93	5.70	2.58
Tb	1.22	.58	.76	.49
Dy	7.52	3.42	3.49	2.81
Ho	1.49	.73	.56	.49
Er	4.06	2.10	1.22	1.20
Tm	.61	.33	.16	.17
Yb	3.83	2.12	.91	1.00
Lu	.54	.33	.14	.14
Y	41.69	20.23	15.74	13.54
Zr	142	105	103	46
Hf	4.41	3.09	3.59	1.73
Nb	22.54	9.93	10.76	10.36
Ta	2.48	.60	.73	1.92
Th	29.68	13.42	22.54	7.51
U	3.33	1.50	4.38	3.38

Geochemistry of (Meta)Granitic Rocks of the West Point Complex and Salcha River Gneiss Dome Areas

Major-, minor-, and trace-element data for the three U-Pb samples and for an undated sample of granitic orthogneiss from the core of the West Point Complex are listed in table 4. The undated sample (98ADb53B, fig. 2) is a weakly foliated, strongly altered, medium-grained, biotite-bearing granitic rock composed of approximately 80 volume percent perthitic K-feldspar with microcline twinning, subordinate plagioclase, quartz, biotite, white mica, and trace amounts of scattered, tiny (approx 0.1 mm diam) garnets, titanite, and Fe-Ti oxides. The rock has a weakly developed fabric defined by a preferred orientation of K-feldspar grains, quartz aggregates, and interstitial, scattered, medium-brown biotite crystals. Much of the biotite is altered to chlorite, and some of the smaller K-feldspar grains are altered to white mica. Quartz in the rock has been annealed, as evidenced by its uniform extinction and straight grain boundaries. Texturally, this rock is similar to the dated granitic orthogneiss, but the abundance of microcline twinning in sample 98ADb53B is similar to that of the dated sample of Devonian augen gneiss (sample 98ADb55B, tables 1, 4).

All four granitic samples have evolved, aluminous and potassic major-element compositions. Unlike the other samples, however, the sample of the granitic dike that intrudes the Salcha River gneiss dome is depleted in all rare-earth elements (La through Lu), as well as in Th, Zr, and Hf (table 4). This relative depletion is likely due to partitioning into accessory minerals, such as allanite and zircon, that remained in the crystal mush from which the melt was segregated. On an Rb-versus-Y+Nb discrimination diagram based on the empirical assignment of granitoids to various tectonic settings, the two samples of West Point orthogneiss and the granitic dike from the Salcha River gneiss dome plot close to one another at the margin of the volcanic-arc field where it adjoins the syncollisional field. The sample of augen gneiss plots along the syncollisional/within-plate boundary but near the apex between these two fields and the volcanic-arc field. All other samples of augen gneiss of known or likely Devonian age in the Lake George assemblage of the Yukon-Tanana Upland similarly plot near the apex of all three fields.

Sample 79AFr2010 of Aleinikoff and others (1984a), from an undeformed granitic stock that intrudes the Salcha River gneiss dome, was previously dated by them at 116±3 Ma. The sample has a major-element composition similar to that of sample 98ADb66B (table 4) but a higher Y content (26 versus 13.54 ppm) and a slightly higher Rb content (216 versus 200 ppm) (Aleinikoff and others, 2000). The Nb content of sample 79AFr2010 is known to be only <10 ppm but probably is similar to that of sample 98ADb66B (10.36 ppm). On this basis, the granitic stock would also plot along the boundary of the syncollisional and volcanic-arc fields, close to sample 98ADb66B. More valuable information, in terms of magma genesis, for the undeformed granitoid is provided by the Pb-, Sr-, O-, and Nd-isotopic data on sample 79AFr2010 determined by Aleinikoff and others (2000, who reported a high $^{207}Pb/^{204}Pb$ ratio (15.72 in K-feldspar), initial $^{87}Sr/^{86}Sr$ ratio (0.74132±0.00009), $\delta^{18}O$ value (11.1 permil), and Σ_{Nd} value (–21.4). These isotopic compositions overlap those expected for intermediate-composition to felsic Paleozoic crust and are consistent with derivation of the granitoid by anatexis of preexisting Yukon-Tanana crust (Aleinikoff and others, 2000), as well as with the abundance of Early Proterozoic inheritance in the igneous zircons, including sample 79AFr2010 and the samples of granitoid orthogneiss and granitic dikes in our study.

Tectonic Implications

The SHRIMP U-Pb zircon data and whole-rock compositional data indicate that the samples of mid-Cretaceous orthogneiss and undeformed granite from the West Point and Salcha River gneiss dome areas, respectively, were largely derived from preexisting continental basement, although the exact tectonic setting in which this magmatism occurred remains uncertain. Blum (1985) proposed that the mid-Cretaceous granitoids in the Fairbanks area were derived from subduction beneath the Yukon-Tanana terrane, whereas Newberry (2000) proposed that the mid-Cretaceous (116–110 Ma) intrusions in interior Alaska represent collisional magmatism. Hansen and Dusel-Bacon (1998) and Dusel-Bacon and others (2002) suggested that the oldest (~115 Ma) mid-Cretaceous plutons may have been emplaced during regional exhumation of higher-grade, lower-plate assemblages after burial by obducted thrust sheets. Evidence that the Salcha River gneiss dome was exposed during this postulated decompression event consists of the presence of andalusite-bearing quartz veins and partial melts within the core of the dome and the permissible closeness of the 113±2-Ma SHRIMP zircon crystallization ages for our granitoid dike sample, the 116±3-Ma TIMS U-Pb zircon age for the adjacent small undeformed intrusion within the dome, and a 113.6±2.8-Ma hornblende $^{40}Ar/^{39}Ar$ cooling age of hornblende-biotite-plagioclase schist from near the proposed detachment between the amphibolite-facies rocks and the overlying greenschist-facies Butte assemblage (see Dusel-Bacon and others, 2002). This geochronologic data set provides a narrow range of Early Cretaceous time during which the metamorphic rocks cooled and, in regard to the West Point orthogneiss, were emplaced and metamorphosed, before intrusion by crosscutting, undeformed granitoids. Ascribing either a metamorphic or igneous origin to the zircon rims in the West Point orthogneiss is compatible with this model because independent evidence suggests a near-contemporaneity for the two events. If our interpretations of the mid-Cretaceous samples and their U-Pb zircon ages are correct, the maximum igneous-crystallization age of the

West Point orthogneiss and the minimum igneous-crystallization age of the posttectonic Salcha intrusion imply that the mid-Cretaceous metamorphic episode occurred between 113 and 111 Ma.

Additional constraints on the timing of metamorphism and posttectonic plutonism in the southeastern part of the Big Delta quadrangle, which may be applicable to the timing of events in the study area (fig. 1), are currently being generated by a comparable SHRIMP U-Pb zircon analysis of amphibolite-grade rocks 75 km to the south, in the Central Creek area, where Day and others (2002) have reported U-Pb ages of 116±4 and 116±2 Ma for what they interpret as metamorphic overgrowths on zircons from a biotite quartzofeldspathic gneiss and a biotite-sillimanite paragneiss, respectively. If correctly interpreted, these ages would appear to date the timing of Cretaceous metamorphism in that area. Day and others have also proposed that this metamorphic event closely preceded the emplacement of undeformed granitic dikes which yielded a SHRIMP U-Pb zircon age of 111±4 Ma.

Whereas the timing of metamorphism and postkinematic plutonism in the West Point and Salcha River gneiss dome areas appears to be similar to that in the Central Creek area in the southeastern part of the Big Delta quadrangle, the sense of shear and the deformational history during the mid-Cretaceous event appear to have differed in these two areas. Day and others (2002) equated this mid-Cretaceous metamorphic episode in their study area with westward-vergent thrusting and observed no evidence of top-to-the-southeast extension. Dusel-Bacon and others' (2002) kinematic study in the Central Creek area also indicated top-to-the-west and top-to-the-northwest structural vergence, with no evidence of the top-to-the-southeast deformation that was equated with crustal extension in the Salcha River gneiss dome area (Pavlis and others, 1993) and in the northeastern Tanacross area, near the Alaska-Yukon Territory border (Hansen and Dusel-Bacon, 1998). Kinematic measurements in the vicinity of the West Point Complex, though sparse, locally indicate top-to-the-southeast vergence (see Oliver and Dusel-Bacon, this volume), which is permissive evidence for the regional extensional event proposed for other parts of the Yukon-Tanana Upland.

Acknowledgments

Charlie Bacon (USGS) played a key role in fieldwork and sample collection. Melanie Hopkins (USGS) provided graphical and office support. Chuck Holdsworth (USGS) expertly separated the zircons from our samples. Brad Ito (USGS) kept the SHRIMP–RG working, and Harold Persing (USGS) provided able all-around assistance with the SHRIMP. Jeff Drake of the University of Alaska, Fairbanks, assisted in the preparation and analysis of mica samples for $^{40}Ar/^{39}Ar$ dating. We thank USGS geologists John Aleinikoff and Dwight Bradley for their helpful reviews of the manuscript.

References Cited

Aleinikoff, J.N., Dusel-Bacon, Cynthia, and Foster, H.L., 1984a, Uranium-lead isotopic ages of zircon from sillimanite gneiss, east-central Alaska, and implications for Paleozoic metamorphism, Big Delta quadrangle, *in* Coonrad, W.L. and Elliott, R.L., eds., The United States Geological Survey in Alaska—accomplishments during 1981: U.S. Geological Survey Circular 868, p. 45–48.

———1986, Geochronology of augen gneiss and related rocks, Yukon-Tanana terrane, east-central Alaska: Geological Society of America Bulletin, v. 97, no. 5, p. 626–637.

Aleinikoff, J.N., Dusel-Bacon, Cynthia, Foster, H.L., and Nokleberg, W.J., 1987, Lead isotopic fingerprinting of tectono-stratigraphic terranes, east-central Alaska: Canadian Journal of Earth Sciences, v. 24, no. 10, p. 2089–2098.

Aleinikoff, J.N., Farmer, G.L., Rye, R.O., and Nokleberg, W.J., 2000, Isotopic evidence for the sources of Cretaceous and Tertiary granitic rocks, east-central Alaska—implications for the tectonic evolution of the Yukon-Tanana terrane: Canadian Journal of Earth Sciences, v. 37, no. 6, p. 945–956.

Aleinikoff, J.N., Foster, H.L., Nokleberg, W.J., and Dusel-Bacon, Cynthia, 1984b, Isotopic evidence from detrital zircons for Early Proterozoic crustal material, east-central Alaska, *in* Coonrad, W.L., and Elliott, R.L., eds., The United States Geological Survey in Alaska—accomplishments during 1981: U.S. Geological Survey Circular 868, p. 43–45.

Aleinikoff, J.N., Moore, T.E., Nokleberg, W.J., and Koch, R.D., 1995, Preliminary U-Pb ages from detrital zircons from the Arctic Alaska and Yukon-Tanana terranes, Alaska [abs.]: Geological Society of America Abstracts with Programs, v. 27, no. 5, p. 2.

Barr, S.M., Raeside, R.P., and van Breemen, Otto, 1987, Grenvillian basement in the northern Cape Breton Highlands, Nova Scotia: Canadian Journal of Earth Sciences, v. 24, no. 5, p. 992–997.

Blum, J.D., 1985, A petrologic and Rb-Sr isotopic study of intrusive rocks near Fairbanks, Alaska: Canadian Journal of Earth Sciences, v. 22, no. 9, p. 1314–1321.

Chatterjee, N.D., and Johannes, Wilhelm, 1974, Thermal stability and standard thermodynamic properties of synthetic $2M_1$-muscovite, $KAl_2(AlSi_3O_{10}(OH)_2)$: Contributions to Mineralogy and Petrology, v. 48, p. 89–114.

Churkin, Michael, Jr., Foster, H.L., Chapman, R.M., and Weber, F.R., 1982, Terranes and suture zones in east-central Alaska: Journal of Geophysical Research, v. 87, no. 5, p. 3718–3730.

Coney, P.J., Jones, D.L., and Monger, W.H., 1980, Cordilleran suspect terranes: Nature, v. 288, no. 5789, p. 329–333.

Creaser, R.A., Heaman, L.M., and Erdmer, Philippe, 1997, Timing of high-pressure metamorphism in the Yukon-Tanana terrane, Canadian Cordillera—constraints from U-Pb zircon dating of eclogite from the Teslin tectonic zone: Canadian Journal of Earth Sciences, v. 34, no. 5, p. 709–715.

Day, W.C., Aleinikoff, J.N., Henning, M.H., Gamble, B.M., and Gough, L.P., 2002, Overview of the bedrock geologic setting of the Big Delta B–2 quadrangle, Alaska [abs.]: Alaska Miners Association Biennial Conference, 18th, Fairbanks, 2002, Abstracts, p. 10–11.

Dusel-Bacon, Cynthia, and Aleinikoff, J.N., 1996, U-Pb zircon and titanite ages for augen gneiss from the Divide Mountain area, eastern Yukon-Tanana upland, Alaska, and evidence for the composite nature of the Fiftymile Batholith, *in* Moore, T.E., and Dumoulin, J.A., eds., Geologic studies in Alaska by the U.S. Geological Survey during 1994: U.S. Geological Survey Bulletin 2152, p. 131–141.

Dusel-Bacon, Cynthia, Brosgé, W.P., Till, A.B., Doyle, E.O., Mayfield, C.F., Reiser, H.N., and Miller, T.P., 1989, Distribution, facies, ages, and proposed tectonic associations of regionally metamorphosed rocks in northern Alaska: U.S. Geological Survey Professional Paper 1497–A, 44 p., 2 sheets, scale 1:1,000,000.

Dusel-Bacon, Cynthia, and Cooper, K.M., 1999, Trace-element geochemistry of metabasaltic rocks from the Yukon-Tanana Upland and implications for the origin of tectonic assemblages in east-central Alaska: Canadian Journal of Earth Sciences, v. 36, no. 10, p. 1671–1695.

Dusel-Bacon, Cynthia, Csejtey, Béla, Jr., Foster, H.L., Doyle, E.O., Nokleberg, W.J., and Plafker, George, 1993, Distribution, facies, ages, and proposed tectonic associations of regionally metamorphosed rocks in east- and south-central Alaska: U.S. Geological Survey Professional Paper 1497–C, 73 p., 2 sheets, scale 1:1,000,000.

Dusel-Bacon, Cynthia, and Foster, H.L., 1983, A sillimanite gneiss dome in the Yukon crystalline terrane, east-central Alaska—petrography and garnet-biotite geothermometry: U.S. Geological Survey Professional Paper 1170–E, 25 p.

Dusel-Bacon, Cynthia, Hansen, V.L., and Scala, J.A., 1995, High-pressure amphibolite facies dynamic metamorphism and the Mesozoic tectonic evolution of an ancient continental margin, east-central Alaska: Journal of Metamorphic Geology, v. 13, no. 1, p. 9–24.

Dusel-Bacon, Cynthia, Lanphere, M.A., Sharp, W.D., Layer, P.W., and Hansen, V.L., 2002, Mesozoic thermal history and timing of structural events for the Yukon-Tanana Upland, east-central Alaska—$^{40}Ar/^{39}Ar$ data from metamorphic and plutonic rocks: Canadian Journal of Earth Sciences, v. 39, no. 6, p. 1013–1051.

Dusel-Bacon, Cynthia, and Murphy, J.M., 2001, Apatite fission-track evidence of widespread Eocene heating and exhumation in the Yukon-Tanana Upland, interior Alaska: Canadian Journal of Earth Sciences, v. 38, no. 8, p. 1191–1204.

Erdmer, Philippe, Ghent, E.D., Archibald, D.A., and Stout, M.Z., 1998, Paleozoic and Mesozoic high-pressure metamorphism at the margin of ancestral North America in central Yukon: Geological Society of America Bulletin, v. 110, no. 5, p. 615–629.

Foster, H.L., 1992, Geologic map of the eastern Yukon-Tanana region, Alaska: U.S. Geological Survey Open-File Report 92–313, 26 p., scale 1:500,000.

Foster, H.L., Cushing, G.W., Keith, T.E.C., and Laird, Jo, 1985, Early Mesozoic tectonic history of the Boundary area, east-central Alaska: Geophysical Research Letters, v. 12, no. 9, p 553–556.

Foster, H.L., Keith, T.E.C., and Menzie, W.D., 1994, Geology of the Yukon-Tanana area of east-central Alaska, *in* Plafker, George, and Berg, H.C., eds., The geology of Alaska, v. G–1 *of* The geology of North America: Boulder, Colo., Geological Society of America, p. 205–240.

Foster, H.L., Laird, Jo, Keith, T.E.C., Cushing, G.W., and Menzie, W.D., 1983, Preliminary geologic map of the Circle quadrangle, Alaska: U.S. Geological Survey Open-File Report 83–170–A, 32 p., scale 1:250,000.

Foster, H.L., Menzie, W.D., Cady, J.W., Simpson, S.L., Aleinikoff, J.N., Wilson, F.H., and Tripp, R.B., 1987, The Alaska Mineral Resource Assessment Program—background information to accompany folio of geologic and mineral resource maps of the Circle quadrangle, Alaska: U.S. Geological Survey Circular 986, 22 p.

Hansen, V.L., 1990, Yukon-Tanana terrane; a partial acquittal: Geology, v. 18, no. 4, p. 365–369.

Hansen, V.L., and Dusel-Bacon, Cynthia, 1998, Structural and kinematic evolution of the Yukon-Tanana upland tectonites, east-central Alaska—a record of late Paleozoic to Mesozoic crustal assembly: Geological Society of America Bulletin, v. 110, no. 2, p. 211–230.

Hansen, V.L., Heizler, M.T., and Harrison, T.M., 1991, Mesozoic thermal evolution of the Yukon-Tanana composite terrane—new evidence from $^{40}Ar/^{39}Ar$ data: Tectonics, v. 10, no. 1, p. 51–76.

Heslop, Kate, Dusel-Bacon, Cynthia, and Williams, I.S., 1995, Survival of zircon U-Pb isotopic systems through partial melting and high P-T dynamothermal metamorphism, Yukon-Tanana terrane, Alaska [abs]: Geological Society of America Abstracts with Programs, v. 27, no. 5, p. 26.

Lanphere, M.A., Dalrymple, G.B., Fleck, R.J., and Pringle, M.S., 1990, Intercalibration of mineral standards for K-Ar and $^{40}Ar/^{39}Ar$ age measurements [abs]: Eos (American Geophysical Union Transactions), v. 71, no. 43, p. 1658.

Layer, P.W., Hall, C.M., and York, Derek, 1987, The derivation of $^{40}Ar/^{39}Ar$ age spectra of single grains of hornblende and biotite by laser step heating: Geophysical Research Letters, v. 14, no. 7, p. 757–760.

Ludwig, K.R., 2001, Users manual for Isoplot/Ex rev. 2.49, a geochronological toolkit for Microsoft Excel: Berkeley, Calif., Berkeley Geochronology Center Special Publication 1a, 56 p.

McDougall, Ian, and Harrison, T.M., 1988, Geochronology and thermochronology by the $^{40}Ar/^{39}Ar$ method: New York, Oxford University Press, 212 p.

Mortensen, J.K., 1992, Pre-mid-Mesozoic tectonic evolution of the Yukon-Tanana terrane, Yukon and Alaska: Tectonics, v. 11, no. 4, p. 836–853.

Newberry, R.J., 2000, Mineral deposits and associated Mesozoic and Tertiary igneous rocks within the interior Alaska and adjacent Yukon portions of the "Tintina gold belt"; a

progress report, *in* Tucker, T.L., and Smith, M.T., chairpersons, The Tintina gold belt; concepts, exploration, and discoveries (special volume 2): Vancouver, British Columbia and Yukon Chamber of Mines, p. 59–87.

Pačes, J.B., and Miller, J.D., 1993, U-Pb ages of the Duluth Complex and related mafic intrusions, northeastern Minnesota: geochronologic insights into physical, paleomagnetic and tectonomagmatic processes associated with the 1.1 Ga mid-continent rift system: Journal of Geophysical Research, v. 98, no. B8, p. 13997–14013.

Pavlis, T.L., Sisson, V.B., Foster, H.L., Nokleberg, W.J., and Plafker, George, 1993, Mid-Cretaceous extensional tectonics of the Yukon-Tanana terrane, Trans-Alaskan Crustal Transect (TACT), east-central Alaska: Tectonics, v. 12, no. 1, p. 103–122.

Pearce, J.A., Harris, N.B.W., and Tindle, A.G., 1984, Trace element discrimination diagrams for the tectonic interpretaton of granitic rocks: Journal of Petrology, v. 25, no. 4, p. 956–983.

Poldervaart, Arie, 1956, Zircons in rocks. 2. Igneous rocks: American Journal of Science, v. 254, no. 9, p. 521–554.

Robinson, M.S., Smith, T.E., and Metz, P.A., 1990, Bedrock geology of the Fairbanks Mining District: Alaska Division of Geological and Geophysical Surveys Professional Report 106, 2 sheets, scale 1:63,360.

Samson, S.D., and Alexander, E.C., Jr., 1987, Calibration of the interlaboratory $^{40}Ar/^{39}Ar$ dating standard, MMhb–1: Chemical Geology, v. 66, no. 1–2, p. 27–34.

Silver, L.T., 1969, A geochronological investigation of the anorthosite complex, Adirondack Mountains, New York, *in* Isachsen, Y.W., ed., Origin of anorthosite and related rocks: New York State Museum and Science Service Memoir 18, p. 233–251.

Smith, T.E., Robinson, M.S., Weber, F.R., Waythomas, C.W., and Reifenstuhl, R.R., 1994, Geologic map of the upper Chena River area, eastern Interior Alaska: Alaska Division of Geological and Geophysical Surveys Professional Report 115, 19 p., scale 1:63,360.

Spear, F.S., 1993, Metamorphic phase equilibria and pressure-temperature-time paths: Washington, D.C., Mineralogical Society of America, 799 p.

Steiger, R.H., and Jäger, Emilie, 1977, Subcommission on geochronology; convention on the use of decay constants in geo- and cosmochronology, Earth and Planet Science Letters, v. 36, no. 3, p. 359–362.

van Breemen, Otto, Davidson, Anthony, Loveridge, W.D., and Sullivan, R.W., 1986, U-Pb zircon geochronology of Grenville tectonites, granulites, and igneous precursors, Parry Sound, Ontario, *in* Moore, J.M., ed., The Grenville Province: Geological Association of Canada Special Paper 31, p. 191–207.

van Breemen, Otto, Henderson, J.B., Loveridge, W.D., and Thompson, P.H., 1987, U-Pb zircon and monazite geochronology and zircon morphology of granulites and granite from the Thelon Tectonic Zone, Healy Lake and Artillery Lake mafic areas, N.W.T., *in* Current research, part A: Geological Survey of Canada Paper 87–1A, p. 783–801.

Weber, F.R., Foster, H.F., Keith, T.E.C., and Dusel-Bacon, Cynthia, 1978, Preliminary geologic map of the Big Delta quadrangle, Alaska. U.S. Geological Survey Open-File Report 78–529–A, scale 1:250,000.

Wheeler, J.O., and McFeely, Patricia, 1991, Tectonic assemblage map of the Canadian Cordillera and adjacent parts of the United States of America: Geological Survey of Canada Map 1712A, scale 1:2,000,000.

Williams, I.S., 1998, U-Th-Pb geochronology by ion microprobe; not just ages but histories, *in* McKibben, M.A., Shanks, W.C., and Ridley, W.I., eds., Applications of microanalytical techniques to understanding mineralizing processes: Society of Economic Geologists Reviews in Economic Geology, v. 7, p. 1–35.

Williams, I.S., and Hergt, J.M., 2000, U-Pb dating of Tasmanian dolerites; a cautionary tale of SHRIMP analysis of high-U zircon, *in* Woodhead, J.D., Hergt, J.M., and Noble, W.P., eds., Beyond 2000; New Frontiers in Isotope Geoscience, Lorne, Australia, Abstracts and Proceedings: Victoria, Australia, University of Melbourne, p. 185–188.

Wilson, F.H., Smith, J.G., and Shew, Nora, 1985, Review of radiometric data from the Yukon crystalline terrane, Alaska and Yukon Territory: Canadian Journal of Earth Sciences, v. 22, no. 4, p. 525–537.

York, Derek, Hall, C.M., Yanase, Yotaro, Hanes, J.A., and Kenyon, W.J., 1981, $^{40}Ar/^{39}Ar$ dating of terrestrial minerals with a continuous laser: Geophysical Research Letters, v. 8, no. 11, p. 1136–1138.